Evaluation of H_2O-CO_2 solubility models in silicate melts: Precision and accuracy of vapor saturation pressure and composition

Ery C. Hughes: University College London (ery.hughes@ucl.ac.uk)

Lee M. Saper: Caltech

This pre-print is not an accepted peer-reviewed manuscript. A version of this pre-print has been submitted to Advances in Geochemistry and Cosmochemistry for peer-review.

Evaluation of H_2O-CO_2 solubility models in silicate melts: Precision and accuracy of vapor saturation pressure and composition

Ery C. Hughes[1,2]* and Lee M. Saper[3]

[1]Department of Earth Sciences, University College London, London, UK

[2]National Isotope Centre, New Zealand Institute for Earth Science Limited, Gracefield, Aotearoa New Zealand

[3]Division of Geological and Planetary Sciences, California Institute of Technology, Pasadena, CA, USA

*Corresponding author: ery.hughes@ucl.ac.uk

Author ORCIDs

Ery C. Hughes: 0000-0002-3445-281X

Lee M. Saper: 0000-0002-3995-9986

Author contributions

Conceptualization: E.C. Hughes, L.M. Saper

Formal Analysis: E.C. Hughes

Investigation: E.C. Hughes

Methodology: E.C. Hughes, L.M. Saper

Visualization: E.C. Hughes

Writing – original draft: E.C. Hughes

Writing – review & editing: E.C. Hughes, L.M. Saper

Data, code, and outputs

The experimental data compilation (no new experimental data is associated with this manuscript); all calculation outputs and figures; and the Jupyter Notebook and Python files for running the

calculations and plotting the figures are available at https://github.com/eryhughes/evaluation_H2O-CO2-solubility-models.

Abstract

Solubility models for H_2O and CO_2 in silicate melt are crucial in igneous petrology and volcanology, in particular for calculating the pressure of vapor saturation of melts from their dissolved volatile content as a barometer, as well as melt and vapor compositions and proportions during degassing. We assessed the accuracy and precision of the calculated pressure of vapor saturation and equilibrium vapor composition using various H_2O-CO_2 solubility models implemented in VESIcal (Dixon, Liu, IaconoMarziano, ShishkinaIdealMixing, and MagmaSat) using a dataset containing 770 vapor-saturated experimental glasses. Experimental and analytical uncertainties were included but model errors were not considered. Across each models' full calibration range, pressure of vapor saturation calculations using IaconoMarziano and MagmaSat are accurate, whilst Dixon, Liu, and ShishkinaIdealMixing, are quite inaccurate, and all are relatively imprecise. Most models except ShishkinaIdealMixing are accurate for vapor composition, but all are relatively imprecise. Both accuracy and precision for each model tend to be better for specific melt compositions within the range of experimental pressure-temperature conditions. Hence, for application to natural systems, it is important to assess the accuracy and precision of H_2O-CO_2 solubility models using experimental data that are closely matched to the system of interest.

Introduction

Water (H_2O) and carbon dioxide (CO_2) are typically the most abundant volatiles in many terrestrial silicate melts prior to extensive degassing or crystallisation (e.g., Edmonds et al., accepted; Wallace, Plank, et al., 2015). The concentration of dissolved volatiles has a major influence on the viscosity and density of magmas; phase equilibria at a given pressure (*P*) and temperature (*T*); and the chemical composition of melt and vapor during degassing (e.g., Dixon & Stolper, 1995; Feig et al., 2006; Giordano et al., 2008). Crucially, the dissolved volatile content of silicate melt is often used as a barometer based on the pressure of vapor saturation (P_{sat}^{v}), often applied to melt inclusion and matrix glass data (e.g., Anderson et al., 1989; Blundy & Cashman, 2008; Hughes et al., 2024). Hence, accurate and precise models of H_2O-CO_2 solubility are critical when trying to petrologically image the plumbing system of a particular volcano or estimate the eruption depth from submarine tephra,

especially if comparing to geophysical estimates (e.g., Hughes et al., 2023; Kilgour et al., 2013; Wieser, Kent, Till, et al., 2023). Additionally, the vapor composition ($x^v_{H_2O}$ and $x^v_{CO_2}$ – mole fraction in the vapor) is often used to calculate the compositions of melt inclusion-hosted bubbles when these bubbles cannot be analysed and therefore to reconstruct the true volatile content of melt inclusions at their time of entrapment (e.g., Rasmussen et al., 2020; Wallace, Kamenetsky, et al., 2015). Water and CO_2 solubility models form the basis of multi-volatile degassing model, which are used to interpret both melt inclusion and volcanic gas data (e.g., Burgisser et al., 2015; Ding et al., 2023; Hughes et al., 2025; Liggins et al., 2020; Moretti et al., 2003; Sun & Lee, 2022). The H_2O content of the melt has a major influence on melt density and viscosity, and therefore H_2O solubility models impact the accuracy of conduit models of volcanic ascent (e.g., La Spina et al., 2022; Mastin, 2002). Accurate CO_2 solubility models are required to estimate magma depth from the C/S ratio of volcanic gases, which is often used in volcano monitoring (e.g., Aiuppa et al., 2007; Kern et al., 2022). Hence, accurate and precise solubilities of H_2O and CO_2 in silicate melts are important for a variety of applications in igneous petrology and volcanology.

In the literature there are a variety of H_2O-CO_2 solubility models, as well as tools for calculating P^v_{sat}, $x^v_{H_2O}$, and $x^v_{CO_2}$ from a specified melt composition using these models (see review by Wieser et al., 2022). Solubility model uncertainties are often assessed by comparing the calculated and measured volatile content of the melt from experiments at known conditions, either graphically or numerically (e.g., Duan, 2014; Ghiorso & Gualda, 2015; Iacono-Marziano et al., 2012; Jiménez-Mejías et al., 2022; Liu et al., 2005; Papale et al., 2022; Shishkina et al., 2014). However, the parameter of interest for users is often the calculated P^v_{sat}, $x^v_{H_2O}$, and/or $x^v_{CO_2}$ from the dissolved H_2O and CO_2, melt composition, and *T*. Hence, sometimes isobars are calculated and graphically compared to experimental data at experimental *P* to assess model accuracy (P_{exp}: e.g., Ghiorso & Gualda, 2015; Jiménez-Mejías et al., 2022; Newman & Lowenstern, 2002; Wieser et al., 2022; Yoshimura, 2023). Occasionally, calculated P^v_{sat} is compared to P_{exp} from experiments graphically (e.g., Duan, 2014;

Newman & Lowenstern, 2002; Papale et al., 2006) or the deviation between them is reported (e.g., Jiménez-Mejías et al., 2022; Papale et al., 2006).

This study builds upon these efforts to investigate the accuracy and precision of existing H_2O-CO_2 solubility models for calculating P_{sat}^{v}, $x_{\text{H}_2\text{O}}^{v}$, and $x_{\text{CO}_2}^{v}$ from the dissolved H_2O and CO_2 content of silicate melt by leveraging: (1) the large number of experiments on H_2O-CO_2 solubility that have been published since 2015, when the most recent of the models used in this study was developed (MagmaSat; Ghiorso & Gualda, 2015), and (2) the creation of the Python package VESIcal (Iacovino et al., 2021) that enables large numbers of calculations of P_{sat}^{v} and equilibrium vapor composition to be done accurately, easily, and quickly using a variety of different H_2O-CO_2 solubility models.

Methods

The aim is to evaluate the accuracy and precision of existing H_2O-CO_2 solubility models by comparing calculated P_{sat}^{v}, $x_{\text{H}_2\text{O}}^{v}$, and $x_{\text{CO}_2}^{v}$ to P_{exp} and measured vapor composition from vapor-saturated melt experiments (e.g., Duan, 2014; Jiménez-Mejías et al., 2022; Newman & Lowenstern, 2002; Papale et al., 2006).

Experimental data in the literature

Experimental data was collated from the literature where there was vapor-saturated silicate melt at known *P* and *T* with measured major/minor oxide, H_2O, and CO_2 concentrations in the quenched glasses. These data mostly come from superliquidus experiments (i.e., melt and vapor only), but some data are from crystallisation experiments. Data collation focussed on studies where the vapor is mixed H_2O-CO_2: however, if experiments on pure-H_2O or -CO_2 with the same melt composition are available, these were also included. If major and minor oxide concentrations are not available for each experimental glass, the average glass composition is used if reported, or, as a last resort, the starting composition was used for superliquidus experiments. As the vapor is assumed to contain only H_2O and CO_2 and the melt only molecular H_2O, hydroxyl ions (OH^-), molecular CO_2,

and/or carbonate ions (CO_3^{2-}) in most models and tools that calculate P_{sat}^{v} and vapor composition, we chose to focus on experiments that are sufficiently oxidising such that H_2, CO, and CH_4 are not important species in the melt or vapor (O_2 is always a small proportion of the vapor phase under geological conditions such that its effect on *P* can be ignored). Additionally, experiments with other volatiles (e.g., Cl and S) were only included if non-H_2O-CO_2 vapor species were a minor component of the vapor. If $x_{\mathrm{H_2O}}^{v}$ and/or $x_{\mathrm{CO_2}}^{v}$ are reported, these are included in the dataset: for mixed H_2O-CO_2 experiments, if only one of $x_{\mathrm{H_2O}}^{v}$ or $x_{\mathrm{CO_2}}^{v}$ are reported, the other is calculated assuming the vapor contains only H_2O and CO_2. If uncertainties are not reported, the following are assumed: ±10 °C for experimental *T* (T_{exp}); ±1% relative for major/minor oxide glass chemistry; and ±10% relative for glass H_2O and CO_2 concentrations.

The collated literature dataset contains 770 individual experimental glasses from 39 studies, covering a wide range of melt compositions and *P*-*T* space (Figure 1; Allison et al., 2019; Behrens et al., 2009; Behrens, Ohlhorst, et al., 2004; Behrens, Tamic, et al., 2004; Blank et al., 1993; Blatter et al., 2013, 2017; Botcharnikov et al., 2005, 2006, 2007; Dixon et al., 1995; Fanara et al., 2015; Fogel & Rutherford, 1990; Hughes et al., 2018; Iacono Marziano et al., 2007; Iacono-Marziano et al., 2012; Iacovino et al., 2013; Jakobsson, 1997; Jendrzejewski et al., 1997; Jiménez-Mejías et al., 2022; King & Holloway, 2002; Lesne, Kohn, et al., 2011; Lesne, Scaillet, Pichavant, & Brey, 2011; Lesne, Scaillet, Pichavant, Iacono-Marziano, et al., 2011; Mangan et al., 2021; Mangan & Sisson, 2000; Melekhova et al., 2017; Pawley et al., 1992; Riker et al., 2015; Schanofski et al., 2019; Shea et al., 2025; Shishkina et al., 2010, 2014; Stanley et al., 2011, 2012; Stolper & Holloway, 1988; Tamic et al., 2001; Vetere et al., 2011, 2014). Most of the experiments were conducted at 800–1300 °C and <10 kbar, with two studies on Martian basalts at 1400–1650 °C and 10–25 kbar (Stanley et al., 2011, 2012) (Figure 1b). Roughly 57 different melt compositions are covered in the dataset: most of the experiments are conducted on basalts/basaltic andesites (36%) and alkali-rich compositions (41%, particularly phonotephrites at 14%), with far fewer on more evolved compositions (6% on andesites, 3% on dacites, and 14% on rhyolites) (Figure 1a and Figure 2). Around 17% have measured Fe^{3+}/Fe_T (Figure 3c), which is sometimes

used in H_2O-CO_2 solubility models (e.g., Ghiorso & Gualda, 2015). Most of the experiments are mixed H_2O-CO_2 (82%), 18% are H_2O-only, and one experiment is CO_2-only (Figure 1c). The maximum H_2O content of the melt is 11.95 wt% and maximum CO_2 is 2.12 wt%, but ~75% of the experiments have <5 wt% H_2O or <3000 ppmw CO_2 (Figure 1c), with 63% of experiments reporting the fluid composition (Figure 3a and b). Just over 30% of the experiments were published since 2015, the year the most recent model tested in this study was published (Ghiorso & Gualda, 2015).

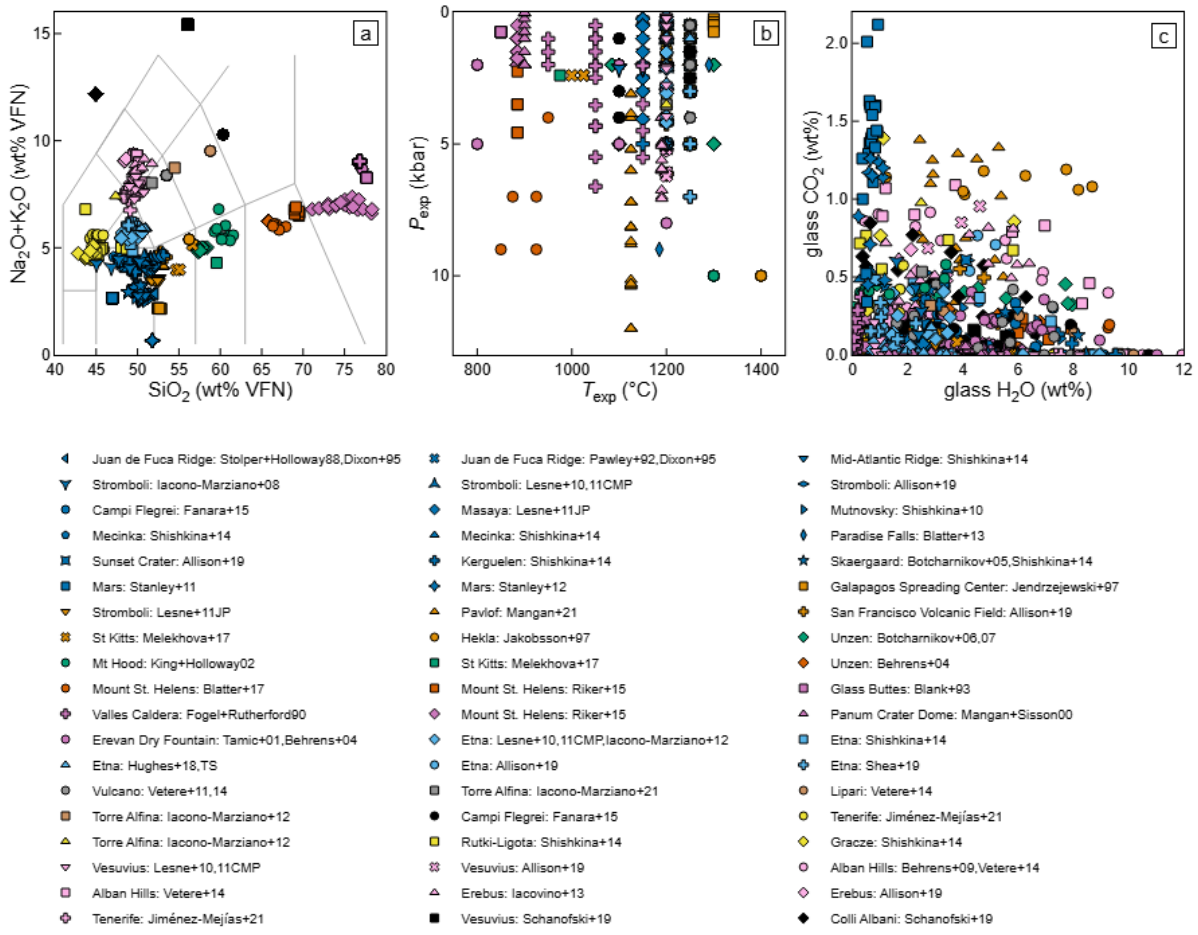

Figure 1: *Glass composition and experimental conditions for vapor-saturated silicate melt experiments collated from the literature (n = 770).* ***(a)*** *Total alkalis (Na_2O+K_2O) vs. SiO_2 (both volatile-free normalised: VFN) with TAS classification fields indicated by grey lines.* ***(b)*** *Experimental pressure (P_{exp}) vs. temperature (T_{exp}): Martian basalts from Stanley et al. (2011) and Stanley et al. (2012), which are at higher P-T, are not shown for clarity.* ***(c)*** *Glass CO_2 vs. H_2O. In all panels, symbol colour indicates the TAS classification and shape (within a TAS classification) indicates specific melt composition (and study/studies) as detailed in the legend. Uncertainties are not plotted for clarity. References: Allison et al. (2019), Behrens et al. (2009), Behrens, Tamic, et al. (2004), Behrens,*

Ohlhorst, et al. (2004), Blank et al. (1993), Blatter et al. (2013), Blatter et al. (2017), Botcharnikov et al. (2005), Botcharnikov et al. (2006), Botcharnikov et al. (2007), Dixon et al. (1995), Fanara et al. (2015), Fogel & Rutherford (1990), Hughes et al. (2018), Iacono Marziano et al. (2007), Iacono-Marziano et al. (2012), Iacovino et al. (2013), Jakobsson (1997), Jendrzejewski et al. (1997), Jiménez-Mejías et al. (2022), King & Holloway (2002), Lesne, Scaillet, Pichavant, & Brey (2011), Lesne, Scaillet, Pichavant, Iacono-Marziano, et al. (2011), Lesne, Kohn, et al. (2011), Mangan & Sisson (2000), Mangan et al. (2021), Melekhova et al. (2017), Pawley et al. (1992), Riker et al. (2015), Schanofski et al. (2019), Shea et al. (2025), Shishkina et al. (2010), Shishkina et al. (2014), Stanley et al. (2011), Stanley et al. (2012), Stolper & Holloway (1988), Tamic et al. (2001), Vetere et al. (2011), and Vetere et al. (2014). All figures were created using Plotly's Python Library.

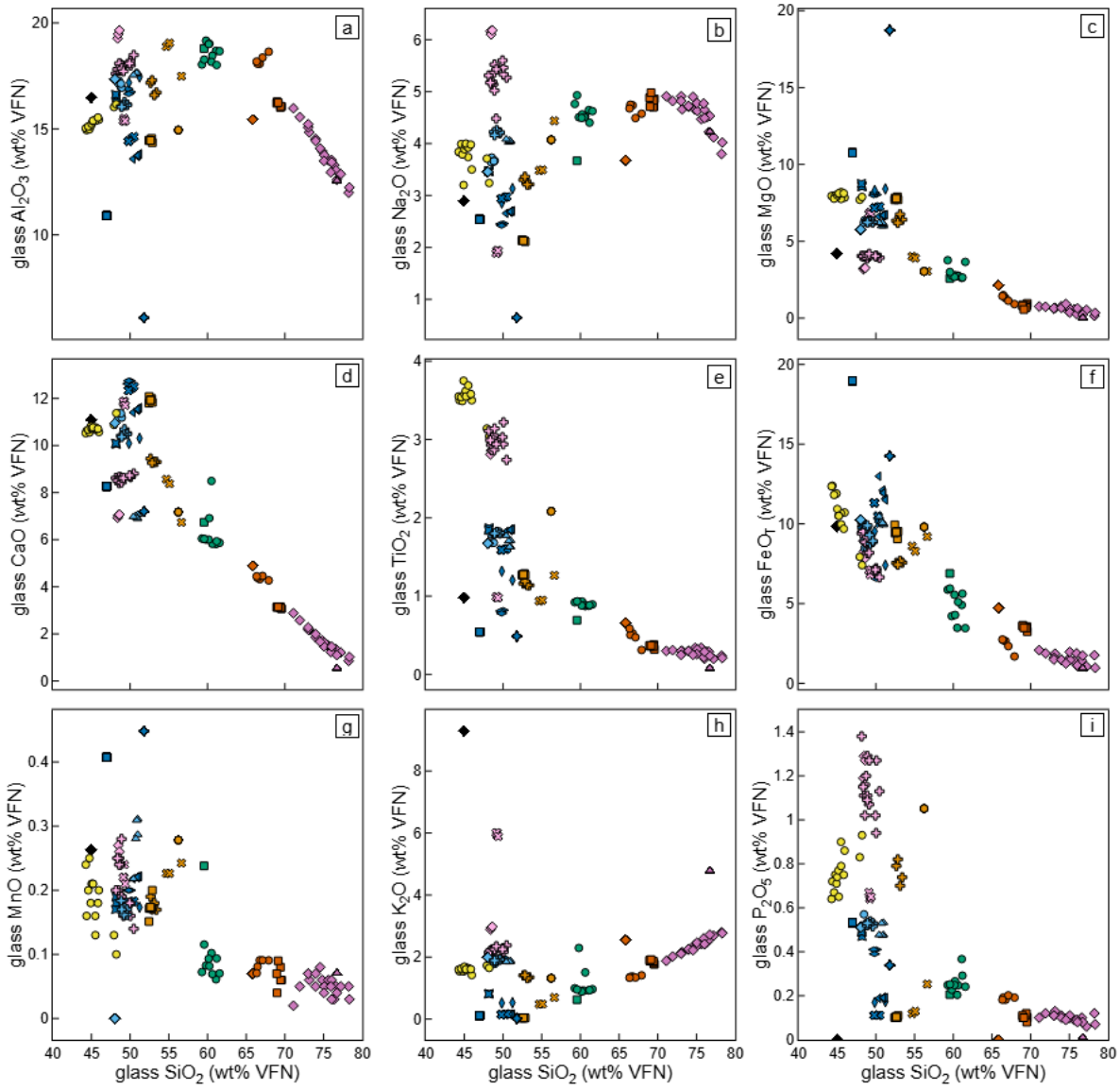

Figure 2: *SiO_2 vs. oxide concentration (both volatile-free normalised, VFN) for all experimental glasses in the dataset. FeO_T refers to total Fe as FeO. Uncertainties are not plotted for clarity. Symbol shapes/colours and references as in Figure 1.*

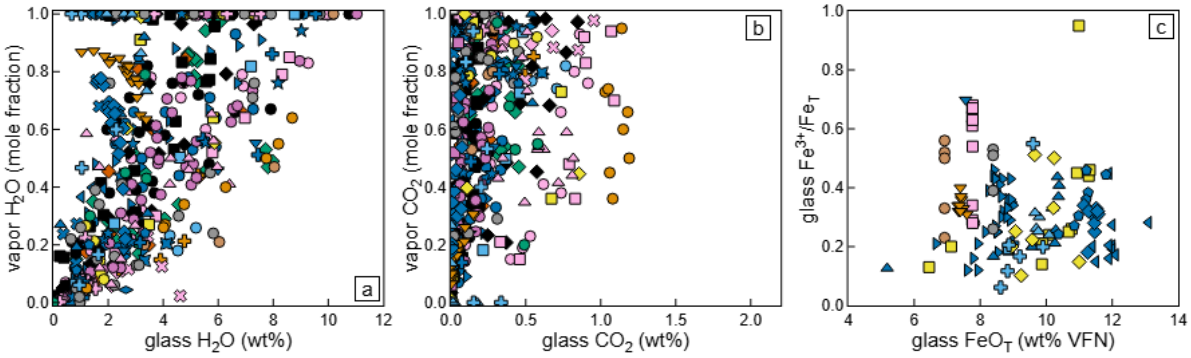

Figure 3: *Vapor composition and iron speciation for experimental glasses in the dataset where it is measured. Vapor composition against glass volatile concentration for* ***(a)*** *H_2O and* ***(b)*** *CO_2.* ***(c)*** *Iron oxidation state (Fe^{3+}/Fe_T) against total iron as FeO in the glass (FeO_T). Uncertainties are not plotted for clarity. Symbol shapes/colours and references as in Figure 1.*

Calculations of the vapor saturation pressure and composition

The Python package VESIcal (v1.2.10, Iacovino et al., 2021) including ThermoEngineLite (v2.0.0.dev7, Wolf et al., 2026) was used to calculate P^v_{sat}, $x^v_{\text{H}_2\text{O}}$, and $x^v_{\text{CO}_2}$ for experiments from the dataset within the reported calibration ranges (Iacovino et al., 2021; Wieser et al., 2022) for the following H_2O-CO_2 solubility models (Table 1 and Figure 4), which are referred to as they are in Iacovino et al. (2021): Dixon (aka VolatileCalc-Basalt: Dixon, 1997; Newman & Lowenstern, 2002); Liu (Liu et al., 2005); IaconoMarziano (Iacono-Marziano et al., 2012); ShishkinaIdealMixing (Shishkina et al., 2014); and MagmaSat (Ghiorso & Gualda, 2015). These models were chosen because they have solubility models for both H_2O and CO_2; are individually applicable to a relatively wide range of melt compositions; are commonly used by the community; are incorporated into external degassing models; and are available in VESIcal that crucially makes conducting tens of thousands of calculations trivial. Broadly, Dixon is applicable to alkali basalts; IaconoMarziano and ShishkinaIdealMixing to sub-alkaline and alkaline basalts through andesites; Liu to rhyolites; and MagmaSat to all natural silicate melts. Given the wealth of experiments containing vapor-saturated silicate melt published since Ghiorso & Gualda (2015), many of the experimental glasses in the dataset were *not* used during calibration of these models, enabling independent evaluation: i.e., data included in a model's calibration are shown

as filled symbols, in Figure 4. Some interpretation was required when deciding if an experiment was included during model calibration due to ambiguities in the original publications.

Table 1: *Calibration range and calculation options for each model.*

Model	*T* (°C)[1]	*P* (bar)[1]	SiO_2 (wt%)[1]	Normalisation[2]	Redox[3]
Dixon	600–1500	<5000	40–49	None	N/A
IaconoMarziano	1100–1400	<10,000	<57.5	Additional	N/A
ShishkinaIdealMixing	1050 – 1400	<5000	<65	Fixed	No
Liu	700–1200	<5000	Rhyolite	Fixed	N/A
MagmaSat	All	All	Natural	Fixed	Yes

Notes: 1 Calibration ranges as described in Iacovino et al. (2021) and Wieser et al. (2022). 2 Melt composition normalisation routine as described in Iacovino et al. (2021), as suggested in Iacovino et al. (2021) and Wieser et al. (2022). 3 Whether Fe^{3+}/Fe_T is used to calculate H_2O-CO_2 solubility within the H_2O-CO_2 solubility model.

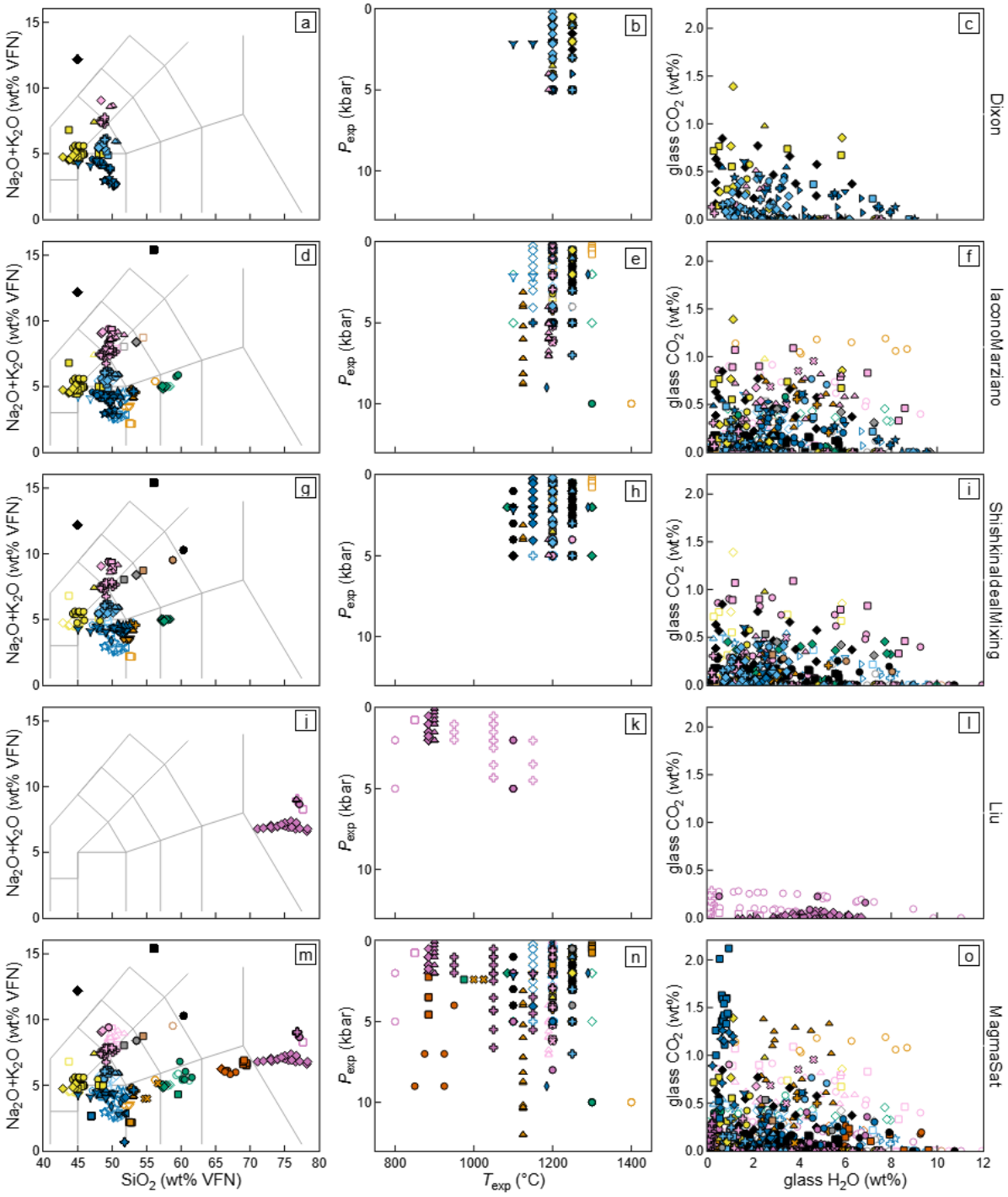

Figure 4: *Glass compositions and experimental conditions for literature experiments used for evaluating H_2O-CO_2 solubility models (labelled on the right-hand side) within their calibration ranges:* ***(a–c)*** *Dixon,* ***(d–f)*** *IaconoMarziano,* ***(g–i)*** *ShishkinaIdealMixing,* ***(j–l)*** *Liu, and* ***(m–o)*** *MagmaSat.* ***(a, d, g, j, m)*** *Total alkalis (Na_2O+K_2O) vs. SiO_2 (both normalised volatile-free: VFN) with TAS classification fields indicated by grey lines.* ***(b, e, h, k, n)*** *Experimental pressure (P_{exp}) vs. temperature (T_{exp}): Martian basalts from Stanley et al. (2011) and Stanley et al. (2012) are not shown for clarity.* ***(c, f, i, l, o)*** *Glass CO_2 vs. H_2O. Symbols, colours, and references as in Figure 1. Uncertainties are not plotted for*

clarity. Open symbols are experiments used to calibrate the model, whereas closed symbols are experiments not used to calibrate the model but within the calibration range of the model (Table 1).

As highlighted in Iacovino et al. (2021) and Wieser et al. (2022), how the glass composition is normalised can affect the results depending on the model. Data was not normalised when using Dixon, as recommended by Wieser et al. (2022); 'additionalvolatiles' was used for IaconoMarziano and 'fixedvolatiles' for MagmaSat as stated in Iacovino et al. (2021); and 'fixedvolatiles' for Liu and ShishkinaIdealMixing (see Iacovino et al., 2021, for definitions of the different normalisation routines; Table 1). The oxidation state of Fe can also effect the results depending on the model (Wieser et al., 2022): Dixon and Liu are unaffected by Fe^{3+}/Fe_T; IaconoMarziano only has an FeO_T term; all Fe is treated as FeO (i.e., FeO_T) for ShishkinaIdealMixing as in the model's calibration; and MagmaSat is sensitive to Fe^{3+}/Fe_T, so measured Fe^{3+}/Fe_T is used where it is reported but all Fe is assumed to be FeO if it is not reported (Table 1).

To include experimental and analytical uncertainty on calculated P_{sat}^{v}, $x_{\text{H}_2\text{O}}^{v}$, and $x_{\text{CO}_2}^{v}$, a Monte Carlo approach using 1000 iterations was applied, except for MagmaSat where 100 iterations were used because it is computationally more expensive and therefore takes longer to run (Iacovino et al., 2021). The composition of each glass (i.e., major/minor oxide, H_2O, and CO_2 concentrations) and T_{exp} were varied within their analytical/experimental uncertainties assuming uncertainties are independent from each other and normally distributed about a specified mean and standard deviation. For each iteration, P_{sat}^{v}, $x_{\text{H}_2\text{O}}^{v}$, and $x_{\text{CO}_2}^{v}$ were calculated using the *calculate_equilibrium_fluid_comp* function in VESIcal, from which the average and standard deviation of each output parameter was calculated and reported for each experimental glass. This unfortunately does *not* include the effect of model uncertainty, which would require varying the model parameters for each H_2O-CO_2 solubility model within their uncertainties, which is not currently implemented in VESIcal (or any available tool), but will be critical to properly assess systematic uncertainties in these models in the future. The normalised error distribution (i.e., [calculated – known]/known) was calculated for P_{sat}^{v}, $x_{\text{H}_2\text{O}}^{v}$, and $x_{\text{CO}_2}^{v}$.

Results

Figure 5 is a comparison of P_{exp} and calculated P_{sat}^{v} (P_{calc}) for each model, whilst measured (where available) and calculated $x_{H_2O}^{v}$ and $x_{CO_2}^{v}$ are shown in Figure 6 and Figure 7, respectively. Both experimental data not included in the calibration of each model but within its calibration range (i.e., filled symbols and bars in Figure 5, Figure 6 and Figure 7), as well as experimental data used for calibrations, are plotted (see Table 2 for number of experiments for each model). Some P_{sat}^{v} values and their uncertainties derived using IaconoMarziano are very large (>10,000 bars P_{sat}^{v} and/or 1000–30,000 bars uncertainty, n = 21), which are all for experiments with 0 ppmw CO_2. These values are not considered further (and are not plotted in Figure 5) because they result from the mathematical limit of the IaconoMarziano model that cannot calculate p_{CO2} = 0 when CO_2 = 0 ppmw (Iacono-Marziano et al., 2012).

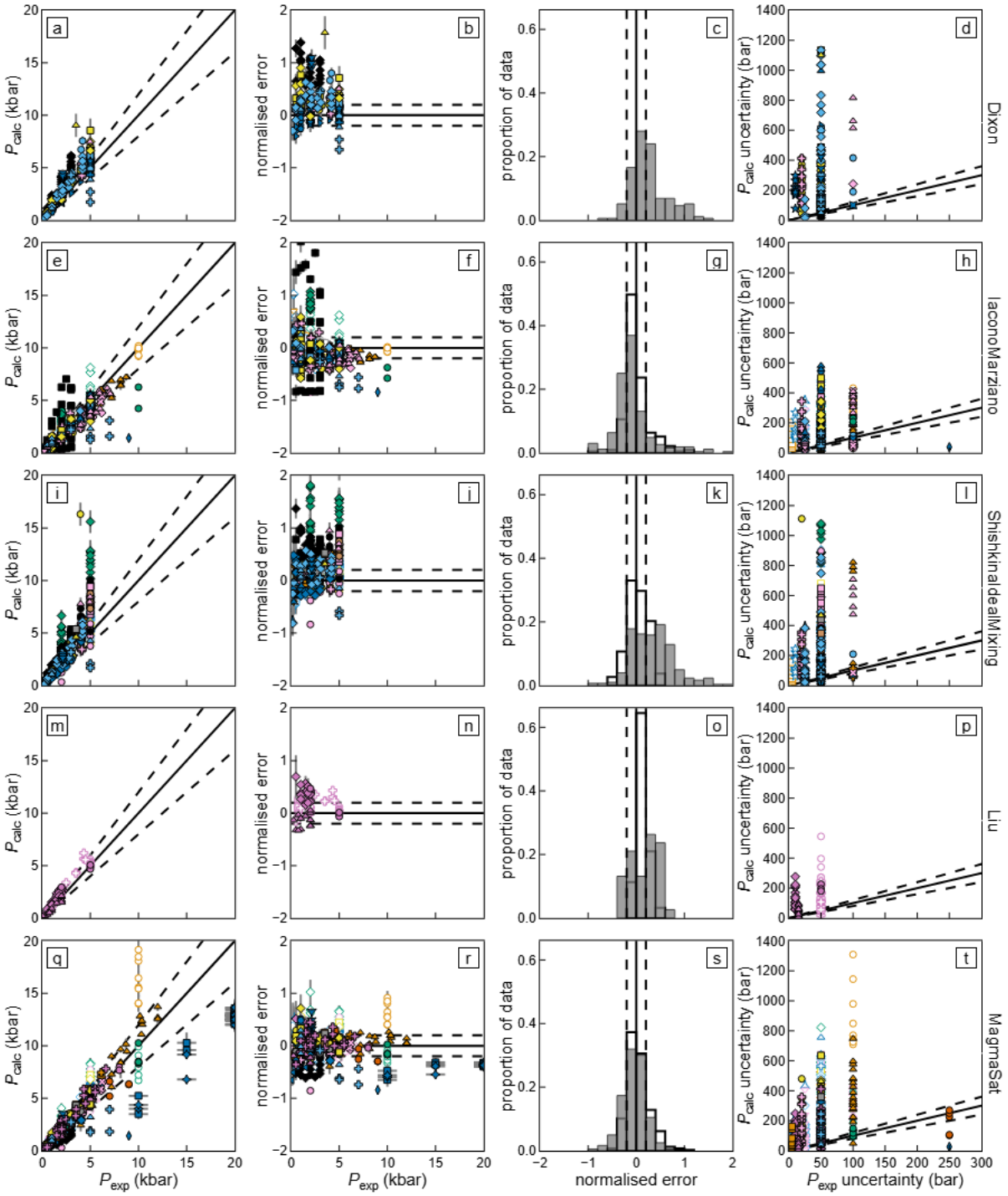

Figure 5: *Evaluating the accuracy and precision of P_{sat}^{v} calculated with H_2O-CO_2 solubility models using VESIcal (labelled along the right-hand side):* ***(a–d)*** *Dixon,* ***(e–h)*** *IaconoMarziano,* ***(i–l)*** *ShishkinaIdealMixing,* ***(m–p)*** *Liu, and* ***(q–t)*** *MagmaSat.* ***(a, e, i, m, q)*** *Calculated P (P_{calc}, i.e., P_{sat}^{v}) vs. experimental P (P_{exp}).* ***(b, f, j, n, r)*** *Normalised error in P_{calc} (i.e., $[P_{calc} - P_{exp}]/P_{exp}$) vs. P_{exp}.* ***(c, g, k, o, s)*** *Histogram of normalised error in P_{calc} by proportion of data.* ***(d, h, l, p, t)*** *Calculated uncertainty in P_{calc} vs. experimental uncertainty in P_{exp} (Martian basalts from Stanley et al. (2011) and Stanley et al. (2012) are not shown as P_{exp} = 1000 bars). In all panels, the black solid line is perfect agreement and*

the black dashed lines are ±20%. Symbols and colours as in Figure 1, except open symbols (or the open bars in the histograms) are data used in calibration of the model, whereas filled symbols (or the grey histograms) are for data not used in calibration of the model.

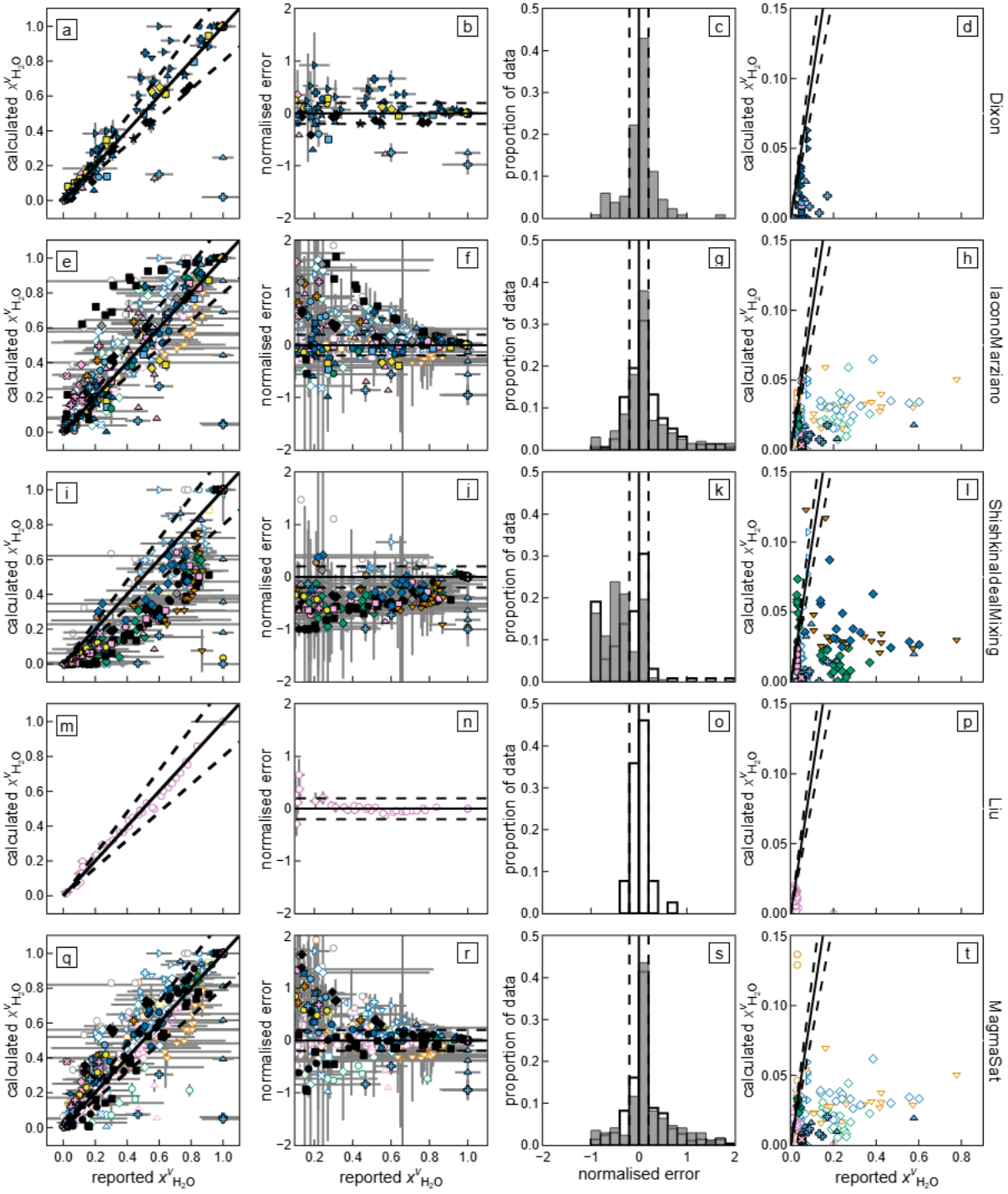

Figure 6: *Evaluating the accuracy and precision of $x^v_{H_2O}$ calculated with H_2O-CO_2 solubility models using VESIcal (labelled along the right-hand side):* ***(a–d)*** *Dixon,* ***(e–h)*** *IaconoMarziano,* ***(i–l)*** *ShishkinaIdealMixing,* ***(m–p)*** *Liu, and* ***(q–t)*** *MagmaSat.* ***(a, e, i, m, q)*** *Calculated $x^v_{H_2O}$ vs. reported*

*$x^v_{H_2O}$. **(b, f, j, n, r)** Normalised error in $x^v_{H_2O}$ (i.e., [calculated $x^v_{H_2O}$ – reported $x^v_{H_2O}$]/reported $x^v_{H_2O}$) vs. reported $x^v_{H_2O}$. **(c, g, k, o, s)** Histogram of normalised error in $x^v_{H_2O}$ by proportion of data. **(d, h, l, p, t)** Calculated uncertainty in calculated $x^v_{H_2O}$ vs. analytical uncertainty in reported $x^v_{H_2O}$ (one value at calculated $x^v_{H_2O}$ uncertainty = 0.35 is excluded in t). In all panels, the black solid line is perfect agreement and the black dashed lines are ±20%. Symbols and colours as in Figure 1 and Figure 5.*

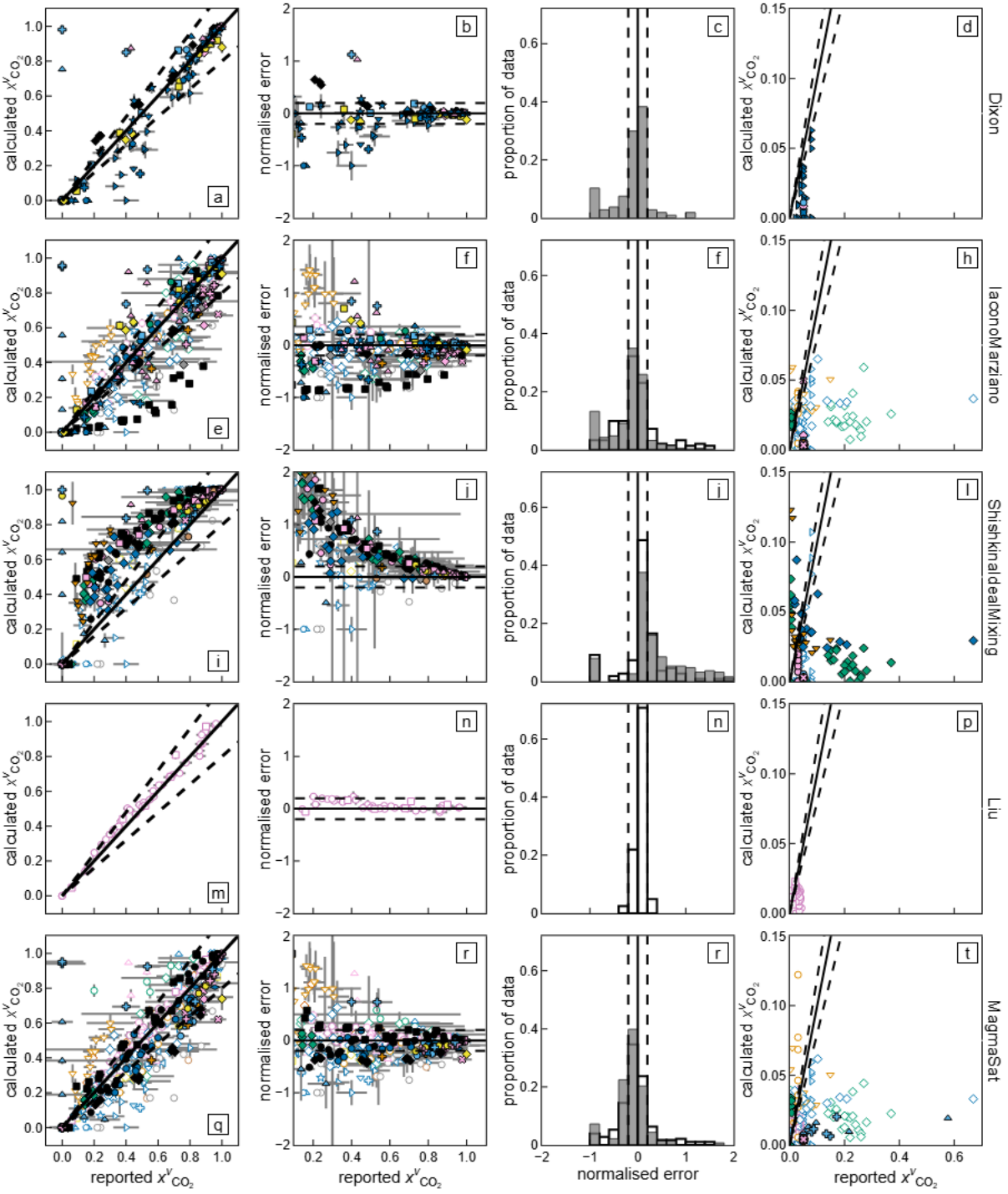

258

259 ***Figure 7****: Evaluating the accuracy and precision of $x^v_{CO_2}$ calculated with H_2O-CO_2 solubility models*
260 *using VESIcal (labelled along the right-hand side):* ***(a–d)*** *Dixon,* ***(e–h)*** *IaconoMarziano,* ***(i–l)***
261 *ShishkinaIdealMixing,* ***(m–p)*** *Liu, and* ***(q–t)*** *MagmaSat.* ***(a, e, i, m, q)*** *Calculated $x^v_{CO_2}$ vs. reported*
262 *$x^v_{CO_2}$.* ***(b, f, j, n, r)*** *Normalised error in $x^v_{CO_2}$ (i.e., [calculated $x^v_{CO_2}$ – reported $x^v_{CO_2}$]/reported $x^v_{CO_2}$) vs.*
263 *reported $x^v_{CO_2}$.* ***(c, g, k, o, s)*** *Histogram of normalised error in $x^v_{CO_2}$ by proportion of data.* ***(d, h, l, p, t)***
264 *Calculated uncertainty in calculated $x^v_{CO_2}$ vs. analytical uncertainty in reported $x^v_{CO_2}$. In all panels, the*

black solid line is perfect agreement and the black dashed lines are ±20%. Symbols and colours as in Figure 1 and Figure 5.

Table 2: *Number of experiments and calculated accuracy and precision of P_{sat}^{v} and $x_{H_2O}^{v}$ across all compositions within each models calibration range.*

Model	Dixon		IaconoMarziano		ShishkinaIdealMixing		Liu		MagmaSat	
P_{sat}^{v}										
n	175	*0*	270	*237*	306	*188*	40	*62*	365	*405*
accuracy (%)	27		-4	*1*	37	*3*	51	*12*	-2	*5*
precision (%)	38		44	*25*	49	*21*	152	*12*	55	*27*
$x_{\mathrm{H_2O}}^{v}$										
n	136	*0*	215	*164*	239	*133*	0	*39*	174	*313*
accuracy (mol.%)	<1		3	*4*	-16	*-5*		*<1*	2	*3*
precision (mol.%)	15		18	*14*	17	*12*		*3*	18	*13*

Notes: Data on experiments not used for calibration are normal type, whereas data for experiments used for calibration are in *italics*.

To evaluate the overall accuracy for each H_2O-CO_2 solubility for P_{sat}^{v}, the mean of the normalised error is compared for experimental data not included for calibration (Table 2 and Figure 8a – the same analyses are reported for experimental data used for calibration for interest, but not discussed). Dixon, ShishkinaIdealMixing and Liu all overestimate P_{sat}^{v} on average by +27–51%; whereas IaconoMarziano and MagmaSat slightly underestimate P_{sat}^{v} by 4 and 2%, respectively (Figure 5c, f, j, n, r, Table 2, and Figure 8a). To evaluate overall precision for each H_2O-CO_2 solubility model, the standard deviation of the normalised error for each model is compared for data not included during model calibration (Table 2 and Figure 8a). The precision of P_{sat}^{v} for all models is poor, ranging between ±38–55% except Liu which is ±152% (Figure 5c, f, j, n, r, Table 2, and Figure 8a). Uncertainties in P_{sat}^{v} incorporating experimental and analytical uncertainties for all models (<1400 bars) are typically much larger than the uncertainty in P_{exp} (typically 20–100 bar: Figure 5 g, k, o, s).

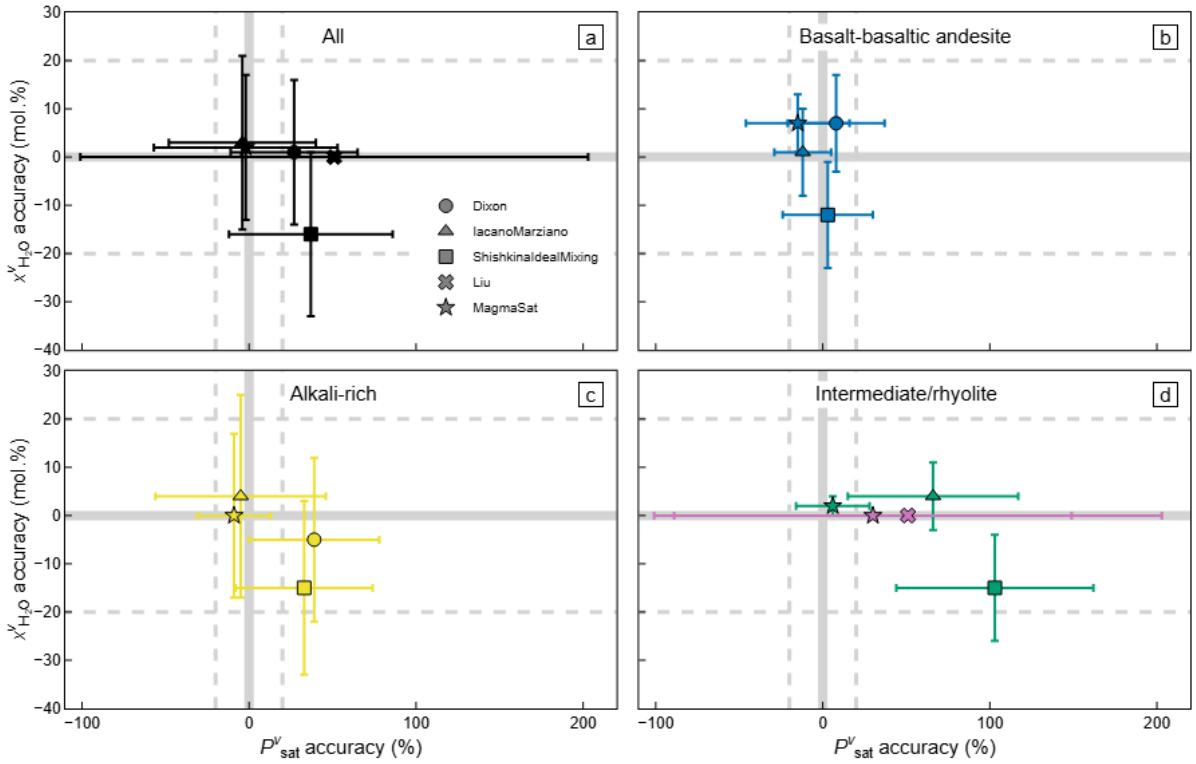

Figure 8: *Comparison of model accuracy and precision for different melt compositions (labelled for each panel): $x^v_{H_2O}$ accuracy vs. P^v_{sat} accuracy, where the error bar indicates precision (based on experiments not used during model calibration):* ***(a)*** *all melt compositions within the calibration range;* ***(b)*** *basalt-basaltic andesites;* ***(c)*** *alkali-rich compositions; and* ***(d)*** *intermediate (green) and rhyolites (pink). Symbol shape indicates model and symbol colour indicates melt composition. The accuracy and precision of $x^v_{H_2O}$ could not be calculated for Liu and MagmaSat for rhyolites due to a lack of experimental data with reported $x^v_{H_2O}$ that was not used to calibrate these models – hence they are arbitrarily plotted at $x^v_{H_2O}$ accuracy = 0 mol.%. The grey solid lines indicate perfect accuracy and the grey dotted lines ±20% accuracy.*

As $x^v_{\mathrm{H_2O}}$ or $x^v_{\mathrm{CO_2}}$ can equal 0, the absolute mean and standard deviation (mol.%) rather than normalised error are compared to evaluate accuracy and precision: values are calculated for $x^v_{\mathrm{H_2O}}$ and assumed to be of similar magnitude (but opposite sign for accuracy) for $x^v_{\mathrm{CO_2}}$ (Table 2 and Figure 8a, although normalised errors are shown in Figure 6 and Figure 7c, f, j, n, and r). For Liu, there is no experimental data with reported $x^v_{\mathrm{H_2O}}$ not used for calibration and therefore independent accuracy and precision cannot be evaluated. Dixon, IaconoMarziano, and MagmaSat have high accuracy (-1 to +3 mol.%), whereas ShishkinaIdealMixing underestimates by 16% (Figure 6, Figure 7, Table 2, and

299 Figure 8a). All models have a similar precision of 15–18 mol.% $x^{v}_{H_2O}$. In contrast to P^{v}_{sat}, uncertainties
300 in calculated $x^{v}_{H_2O}$ and $x^{v}_{CO_2}$ are typically smaller than measurement uncertainties (<15 vs. <100
301 mol.%; Figure 6 and Figure 7g, k, o, s).

302 Discussion

303 Overall, IaconoMarziano and MagmaSat are accurate for P^{v}_{sat} within their calibration range (-4
304 and -2%, respectively), whilst the other models are quite inaccurate (+30–50%) and the precision for
305 all models is quite poor for P^{v}_{sat} (38–151%) (Table 2 and Figure 8a). Because H_2O and CO_2 solubility
306 models are equations that calculate the concentration of H_2O and CO_2 under a set of conditions, the
307 uncertainties in these models are typically quoted in reference to how well the models reproduce
308 the measured H_2O and CO_2 concentrations of experiments, which are normally ±10–20% precision:
309 Dixon: 8–15 % for H_2O and ~15% for CO_2 and (Dixon, 1997; Duan, 2014); IaconoMarziano: average
310 error for H_2O is 8–17% and CO_2 is 12–13% (Duan, 2014; Iacono-Marziano et al., 2012);
311 ShishkinaIdealMixing: 78% are within ±10% for H_2O and 70% are within 20% for CO_2 (Shishkina et al.,
312 2014); Liu: 6–8% for H_2O and 10–26% for CO_2 (Duan, 2014; Liu et al., 2005); and MagmaSat: ~25% for
313 H_2O and ~10% for CO_2 (Ghiorso & Gualda, 2015). The poorer precision in P^{v}_{sat} compared to replicating
314 the dissolved H_2O and CO_2 concentrations highlights that uncertainties in both H_2O and CO_2 solubility
315 contribute to uncertainty in P^{v}_{sat}. The accuracy in vapor composition is good for most models (1–3
316 mol.%), except ShishkinaIdealMixing (16 mol.%), but precision is quite poor (15–18 mol.%).
317 Unfortunately, this highlights that previous models are not particularly accurate (Dixon,
318 ShishkinaIdealMixing, Liu) and/or precise (all models) in predicting P^{v}_{sat} or the vapor composition
319 even within their stated calibration ranges (Figure 8a).

320 Accuracy and precision for different melt compositions

321 The accuracy and precision of different H_2O-CO_2 solubility models may differ for different
322 compositions within their calibration ranges, which are reported for basalt-basaltic andesites, alkali-
323 rich, intermediates, and rhyolites in Table 3 and Figure 8b–d. Basalt-basaltic andesite melts are very

common across a wide variety of tectonic settings and are relatively well represented in the experimental dataset (Figure 4). For basalt-basaltic andesites (Table 3 and Figure 9b), the accuracy and precision in P^{v}_{sat} improves significantly compared to the full calibration range for Dixon and ShishkinaIdealMixing (8/29 and 3/27% for accuracy/precision, respectively), whereas for IaconoMarziano and MagmaSat the accuracy reduces slightly (-12 to -15%), but the precision improves (31 to 17%). There are slight improvements in the accuracy of $x^{v}_{\mathrm{H_2O}}$ for IaconoMarziano, ShishkinaIdealMixing, and MagmaSat, but the accuracy for Dixon gets worse (7 mol.%). Precision in $x^{v}_{\mathrm{H_2O}}$ improves for Dixon, IaconoMarziano, and ShishkinaIdealMixing (10–11 mol.%) and remains similar for MagmaSat. Overall, for all models, accuracy and precision in P^{v}_{sat} and $x^{v}_{\mathrm{H_2O}}$ (except P^{v}_{sat} accuracy for IaconoMariziano and MagmaSat) are better for basalt-basaltic andesites compared to their full calibration ranges (Figure 8a and b).

Table 3: *Number of experiments and calculated accuracy and precision of P^{v}_{sat} and $x^{v}_{H_2O}$ for difference melt compositions.*

Model	Dixon		IaconoMarziano		ShishkinaIdealMixing		Liu		MagmaSat	
Basalt-basaltic andesite										
P^{v}_{sat} *n*	55	*0*	64	*89*	37	*94*	0	*0*	83	*125*
P^{v}_{sat} accuracy (%)	8		-12	*-4*	3	*-1*			-15	*1*
P^{v}_{sat} precision (%)	29		17	*25*	27	*23*			31	*21*
$x^{v}_{\mathrm{H_2O}}$ *n*	52	*0*	53	*65*	19	*76*	0	*0*	31	*107*
$x^{v}_{\mathrm{H_2O}}$ accuracy (mol.%)	7		1	*7*	-12	*-6*			7	*9*
$x^{v}_{\mathrm{H_2O}}$ precision (mol.%)	10		9	*11*	11	*12*			6	*11*
Alkali-rich										
P^{v}_{sat} *n*	98	*0*	155	*57*	204	*35*	0	*0*	149	*134*
P^{v}_{sat} accuracy (%)	39		-5	*-6*	33	*5*			-9	*4*
P^{v}_{sat} precision (%)	39		51	*15*	41	*17*			22	*18*
$x^{v}_{\mathrm{H_2O}}$ *n*	67	*0*	134	*20*	161	*14*	0	*0*	131	*68*
$x^{v}_{\mathrm{H_2O}}$ accuracy (mol.%)	-5		4	*-2*	-15	*-9*			<1	*1*
$x^{v}_{\mathrm{H_2O}}$ precision (mol.%)	17		21	*7*	18	*11*			17	*13*
Intermediate										
P^{v}_{sat} *n*	0	*0*	13	*22*	37	*0*	0	*0*	28	*46*
P^{v}_{sat} accuracy (%)			66	*34*	103				-6	*3*

P^v_{sat} precision (%)			51	*25*	59				22	*26*
$x^v_{H_2O}$ *n*	0	*0*	13	*22*	37	*0*	0	*0*	8	*46*
$x^v_{H_2O}$ accuracy (mol%)			4	*10*	-15				2	*-4*
$x^v_{H_2O}$ precision (mol%)			7	*15*	11				2	*14*
Rhyolite										
P^v_{sat} *n*	0	*0*	0	*0*	0	*0*	40	*62*	60	*47*
P^v_{sat} accuracy (%)							51	*12*	30	*1*
P^v_{sat} precision (%)							152	*12*	119	*12*
$x^v_{H_2O}$ *n*	0	*0*	0	*0*	0	*0*	0	*39*	0	*39*
$x^v_{H_2O}$ accuracy (mol%)								*<1*		*<1*
$x^v_{H_2O}$ precision (mol%)								*3*		*4*

Notes: Data for experiments not used for calibration are normal type, whereas data for experiments used for calibration are in *italics*.

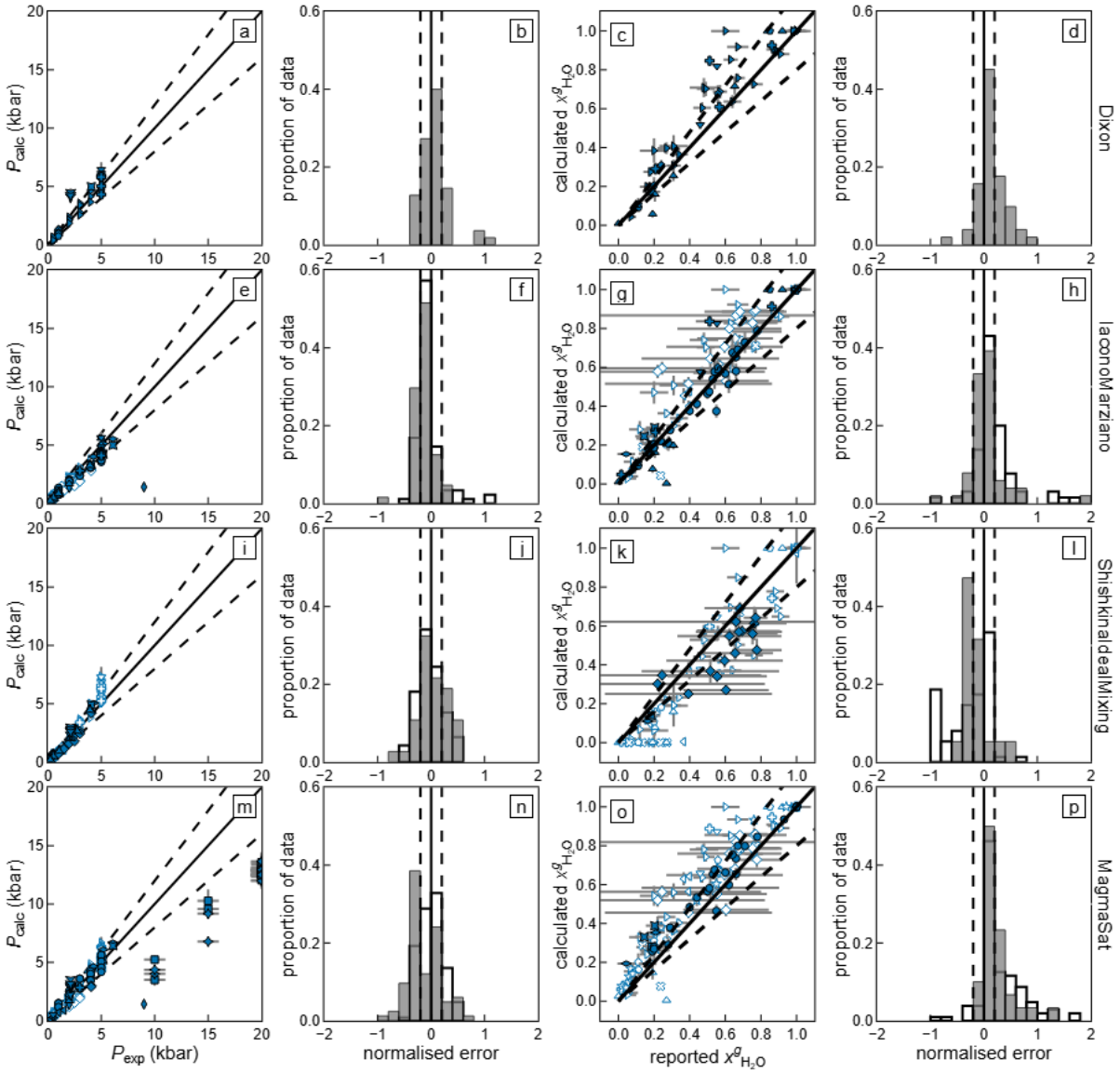

Figure 9: *Evaluating the accuracy and precision of P^v_{sat} and $x^v_{H_2O}$ calculated with H_2O-CO_2 solubility models using VESIcal (labelled along the right-hand side) for basalt and basaltic andesite melts:* ***(a–d)*** *Dixon,* ***(e–h)*** *IaconoMarziano,* ***(i–l)*** *ShishkinaIdealMixing, and* ***(m–p)*** *MagmaSat.* ***(a, e, i, m)*** *Calculated P (P_{calc}, i.e., P^v_{sat}) vs. experimental P (P_{exp}).* ***(b, f, j, n)*** *Histogram of normalised error in P_{calc} by proportion of data.* ***(c, g, k, o)*** *Calculated $x^v_{H_2O}$ vs. reported $x^v_{H_2O}$.* ***(d, h, l, p)*** *Histogram of normalised error in $x^v_{H_2O}$ by proportion of data. In all panels, the black solid line is perfect agreement and the black dashed lines are ±20%. Symbols and colours as in Figure 1 and Figure 5.*

Alkali-rich melts have been targeted experimentally due to being present at a quite a few well-studied volcanoes and their large effect on CO_2-solubility. For alkali-rich melts (Table 3 and Figure 10), the precision is similar but the accuracy worse for both P^v_{sat} and $x^v_{H_2O}$ for Dixon (accuracy drops to 39% and -5 mol.%, respectively). IaconoMariziano has similar accuracy but slightly worse precision

for both P^{v}_{sat} and $x^{v}_{\mathrm{H_2O}}$. For ShishkinaIdealMixing, the precision and accuracy of P^{v}_{sat} are slightly better for alkali-rich melts, and similar for $x^{v}_{\mathrm{H_2O}}$. Precision and accuracy of $x^{v}_{\mathrm{H_2O}}$ are the same for MagmaSat, similar for P^{v}_{sat} accuracy, but there is a marked improvement for P^{v}_{sat} precision (down to 22%). Overall, alkali-rich melts are well reproduced by IaconoMarziano and ShishkinaIdealMixing, and particularly well by MagmaSat (Figure 8a and c).

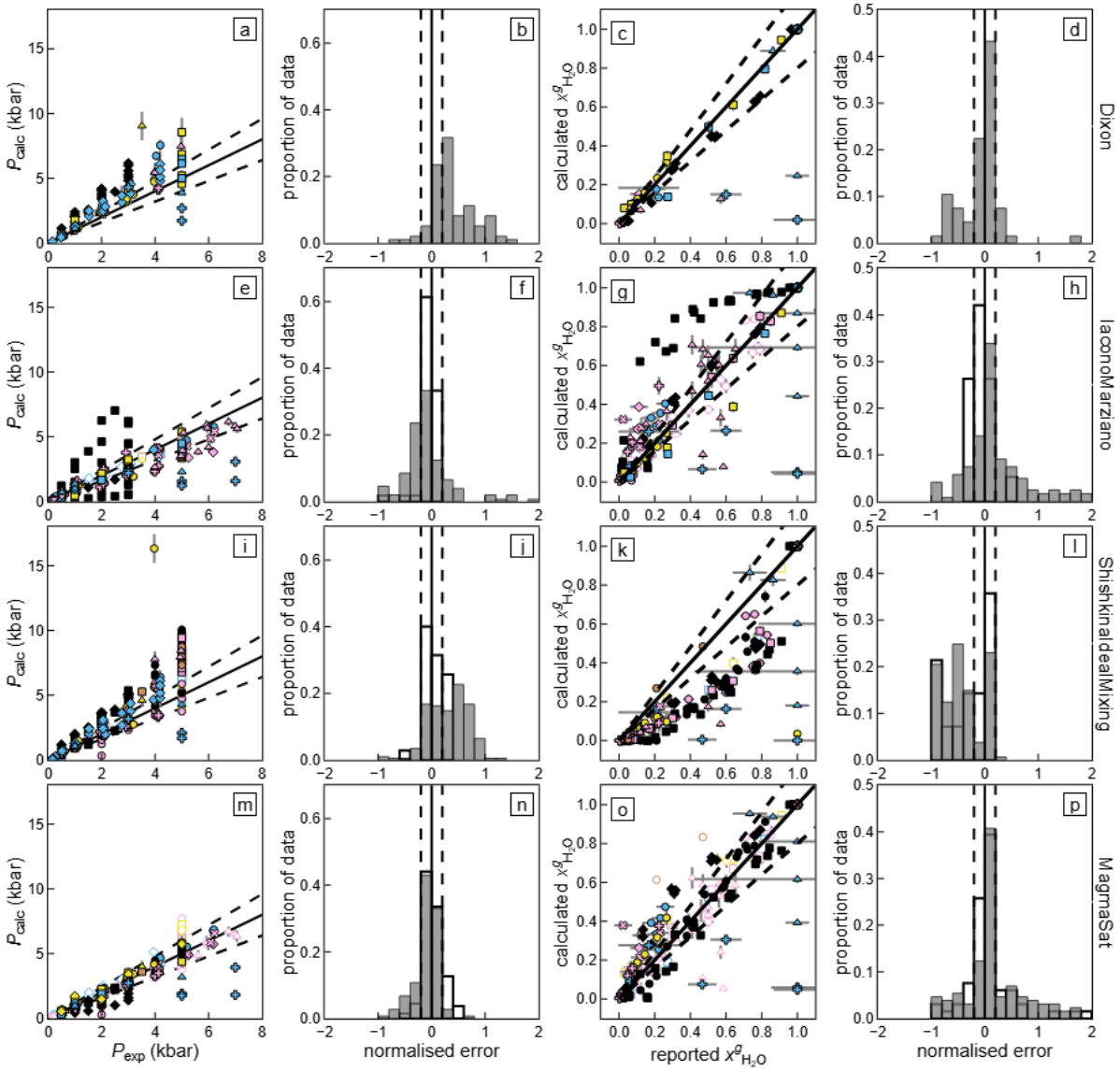

Figure 10: *Evaluating the accuracy and precision of P^{v}_{sat} and $x^{v}_{H_2O}$ calculated with H_2O-CO_2 solubility models using VESIcal (labelled along the right-hand side) for alkali-rich melts:* ***(a–d)*** *Dixon,* ***(e–h)*** *IaconoMarziano,* ***(i–l)*** *ShishkinaIdealMixing, and* ***(m–p)*** *MagmaSat.* ***(a, e, i, m)*** *Calculated P (P_{calc}, i.e., P^{v}_{sat}) vs. experimental P (P_{exp}).* ***(b, f, j, n)*** *Histogram of normalised error in P_{calc} by proportion of data.* ***(c, g, k, o)*** *Calculated $x^{v}_{H_2O}$ vs. reported $x^{v}_{H_2O}$.* ***(d, h, l, p)*** *Histogram of normalised error in $x^{v}_{H_2O}$ by*

proportion of data. In all panels, the black solid line is perfect agreement and the black dashed lines are ±20%. Symbols and colours as in Figure 1 and Figure 5.

Wieser et al. (2022) explored the accuracy of H_2O-CO_2 solubility models for intermediate (andesite and dacite) melts given their dominance in subduction zones and hazardous volcanoes. Wieser et al. compared isobars calculated using various models through VESIcal and Solwcad (Papale et al., 2006) with P_{exp} (their Figure 16) and concluded MagmaSat was the most accurate model, predicting volatiles contents within ±20% of reported values. For intermediate melts (Table 3 and Figure 11), the accuracy and precision of P_{sat}^{v} is much worse for IaconoMarziano and ShishkinaIdealMixing (66–100% accuracy), but there are slight improvements in $x_{\mathrm{H_2O}}^{v}$ precision and accuracy compared to their full calibration range. The accuracy of P_{sat}^{v} and $x_{\mathrm{H_2O}}^{v}$ are slightly worse for MagmaSat compared to its full calibration, but the precision is better (22% for P_{sat}^{v}). Overall, as suggested by Wieser al. (2022), MagmaSat has the best accuracy and precision for intermediate melts (Figure 8d). However, the lack of experimental studies on intermediate melts severely limits the applicability of any H_2O-CO_2 solubility model to such magmas due to a lack of calibration data (e.g., Wieser et al., 2022). Interestingly, there are a large number of experimental studies investigating vapor-saturated calc-alkaline intermediate magmas in the literature that have unfortunately not measured H_2O and/or CO_2 in the glass (e.g., Alonso-Perez et al., 2008; Blatter et al., 2023; Blatter & Carmichael, 1998; Krawczynski et al., 2012; Marxer et al., 2021; Nandedkar et al., 2014). These (and new) experiments could fill crucial gaps in H_2O and/or CO_2 solubility model compositional space in the future.

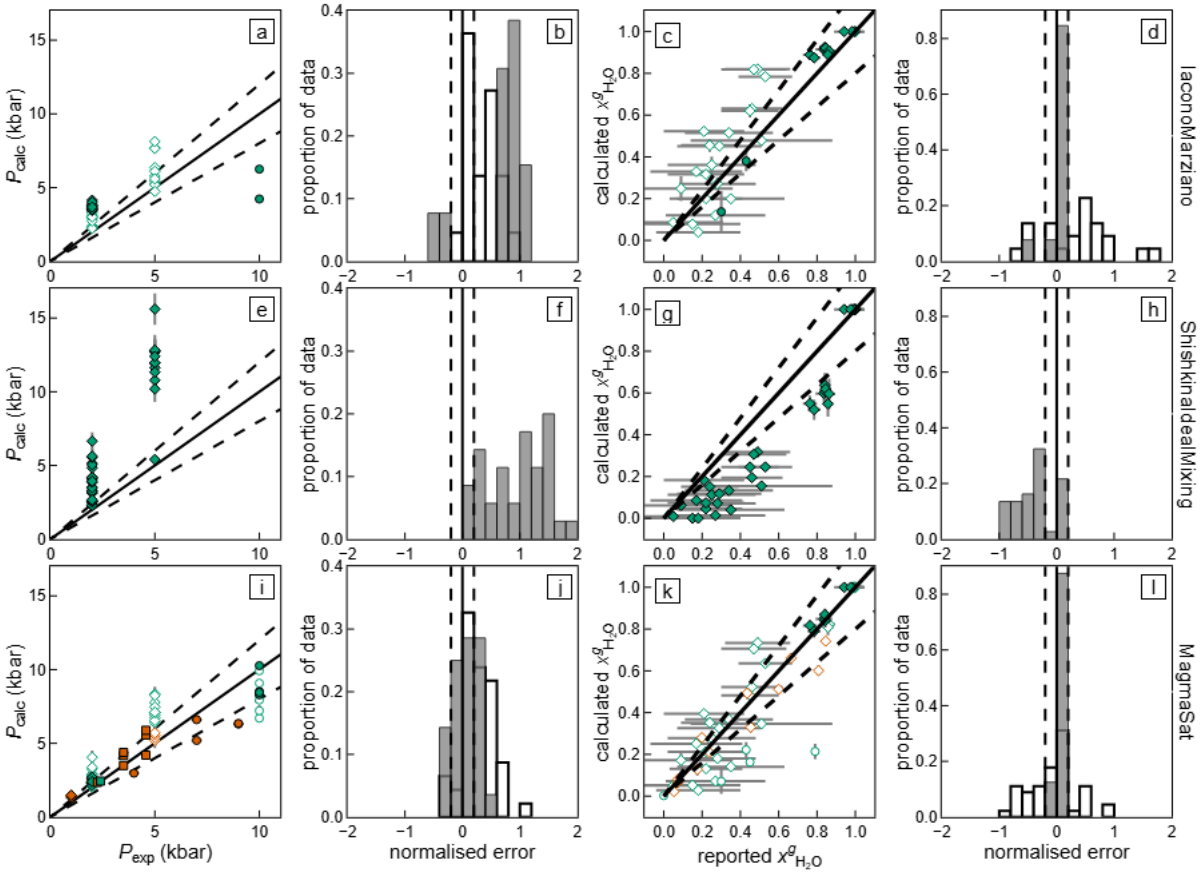

Figure 11: *Evaluating the accuracy and precision of P^v_{sat} and $x^v_{H_2O}$ calculated with H_2O-CO_2 solubility models using VESIcal (labelled along the right-hand side) for intermediate (andesite and dacite) melts:* ***(a–d)*** *IaconoMarziano,* ***(e–h)*** *ShishkinaIdealMixing, and* ***(i–l)*** *MagmaSat.* ***(a, e, i)*** *Calculated P (P_{calc}, i.e., P^v_{sat}) vs. experimental P (P_{exp}).* ***(b, f, j)*** *Histogram of normalised error in P_{calc} by proportion of data.* ***(c, g, k)*** *Calculated $x^v_{H_2O}$ vs. reported $x^v_{H_2O}$.* ***(d, h, l)*** *Histogram of normalised error in $x^v_{H_2O}$ by proportion of data. In all panels, the black solid line is perfect agreement and the black dashed lines are ±20%. Symbols and colours as in Figure 1 and Figure 5.*

For rhyolites (Table 3 and Figure 12), only the accuracy and precision of P^v_{sat} can be evaluated as all experimental data with reported vapor composition was used for calibrating both Liu and MagmaSat. P^v_{sat} accuracy and precision are much worse for MagmaSat compared to the whole calibration range (31% and 119%, respectively), which likely reflects the low pressure of these experiments and therefore large relative errors for small absolute differences.

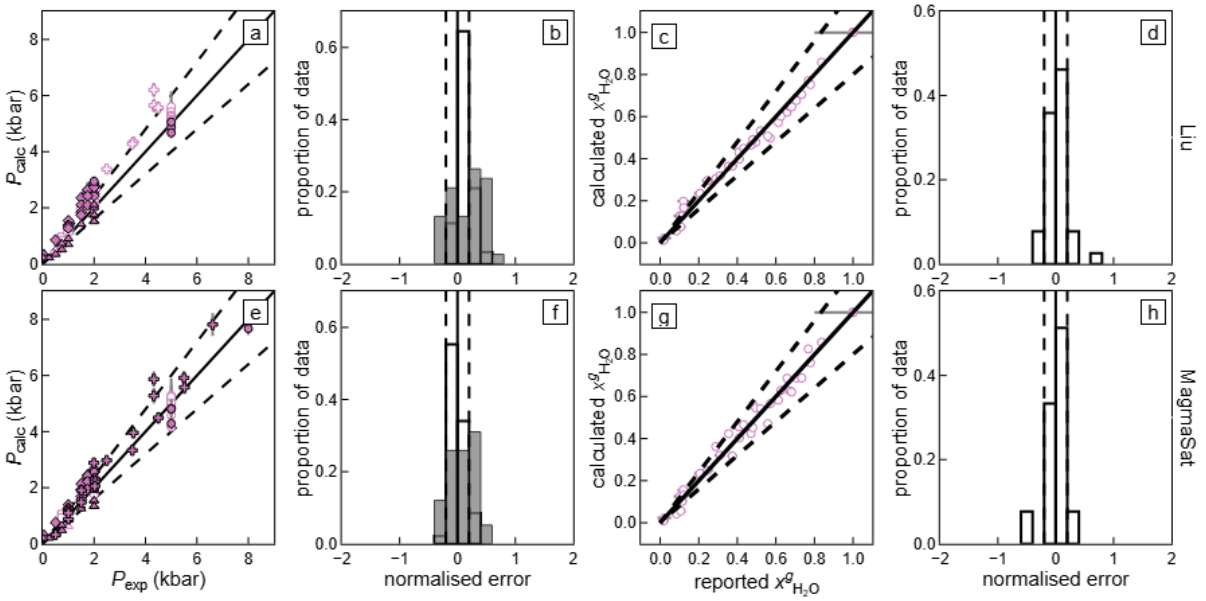

Figure 12: *Evaluating the accuracy and precision of P^v_{sat} and $x^v_{H_2O}$ calculated with H_2O-CO_2 solubility models using VESIcal (labelled along the right-hand side) for rhyolite melts:* ***(a–d)*** *Liu and* ***(e–h)*** *MagmaSat.* ***(a, e)*** *Calculated P (P_{calc}, i.e., P^v_{sat}) vs. experimental P (P_{exp}).* ***(b, f)*** *Histogram of normalised error in P_{calc} by proportion of data.* ***(c, g)*** *Calculated $x^v_{H_2O}$ vs. reported $x^v_{H_2O}$.* ***(d, h)*** *Histogram of normalised error in $x^v_{H_2O}$ by proportion of data. In all panels, the black solid line is perfect agreement and the black dashed lines are ±20%. Symbols and colours as in Figure 1 and Figure 5.*

This approach of calculating the accuracy and prevision of P^v_{sat} and vapor composition can be used to evaluate how well existing solubility models reproduce new experimental data in the future and can be repeated on new H_2O-CO_2 solubility models as they are published to ensure the best estimates of accuracy and precision are available. Given ~30% of the experimental dataset was published after these models were published, improved H_2O-CO_2 solubility models may be possible using these 'new' data.

Influence of analytical uncertainty

Using a Monte Carlo approach to incorporate experimental uncertainty in T_{exp} and analytical uncertainty in glass composition (majors/minors, H_2O, and CO_2) enables a comparison between the uncertainties in experimental *P* and the precision in calculated P^v_{sat}, and the analytical uncertainties in measured and precision in calculated vapor composition, for an individual glass measurement (i.e.,

what is the spread in calculated P_{sat}^{v} and vapor composition due to experimental and analytical uncertainties). This is a minimum estimate in the precision in calculated P_{sat}^{v} and vapor composition for an individual glass composition because model uncertainty is not included. Calculated P_{sat}^{v} precision for an individual experimental glass composition is typically larger than experimental uncertainty in P_{exp} (Figure 5g, k, o, s). This suggests improved precision in P_{sat}^{v} for natural samples (e.g., melt inclusions and matrix glass) will require reduced uncertainties in measured H_2O and CO_2. However, similar uncertainties in measured H_2O and CO_2 exist in the calibration datasets for the H_2O-CO_2 solubility models themselves, which would be reflected in model error. Conversely, calculated precision in vapor composition from an individual glass composition is typically better than analytical uncertainty (Figure 6 and Figure 7g, k, o, s), highlighting the analytical challenges of measuring experimental vapor composition.

A similar Monte Carlo approach can be applied to natural sample data to account for analytical uncertainty in calculated P_{sat}^{v} and vapor composition (e.g., Hughes et al., 2025). Inclusion of analytical uncertainties will result in worse calculated precision for natural samples (i.e., melt inclusions and matrix glasses) than the experimental glasses explored here (assuming melt inclusion compositions at entrapment can be faithfully reconstructed: Rose-Koga et al., 2021). Firstly, for these experiments, *T* is known with a small uncertainty (e.g., ±10 °C), whereas for natural samples, *T* is not known independently and is typically calculated from the glass composition, which is associated with larger uncertainties (e.g., >30 °C depending on the thermometer; Wieser et al., 2025). This is likely to cause a small change in the calculated precision because H_2O-CO_2 solubility is typically not strongly *T*-dependent (e.g., Wieser et al., 2022). Secondly, for melt inclusions, CO_2 is often hosted in a vapor bubble in addition to the glass (e.g., Hartley et al., 2014; Moore et al., 2015; Wallace, Kamenetsky, et al., 2015), which leads to larger analytical uncertainties in CO_2 compared to experiments (see Wieser et al. (2025) for a discussion on this topic). Thirdly, uncertainties in the melt composition will be larger for melt inclusions where corrections for post-entrapment crystallisation and melting have

been applied (although the difference in calculated P_{sat}^{v} is small when these corrections are included: van Gerve et al., 2025).

Using experimental data to select the most appropriate model

Ultimately, users of H_2O-CO_2 solubility models wish to use the model that will produce the most accurate and precise results for their application of interest – whether that is calculating the composition of vapor bubbles in melt inclusions to reconstruct the true dissolved volatile content at entrapment; P_{sat}^{v} from melt inclusion or matrix glass data to estimate magma storage or eruption depth; or the melt and vapor compositions and proportions during degassing to compare to natural data or as an input to conduit flow models. Comparison to the calibration dataset for a model is typically the first step in choosing the most appropriate model (e.g., Iacovino et al., 2021). However, the accuracy and precision of the H_2O-CO_2 solubility models explored here must also be taken into consideration when making inferences about natural systems and comparison to other datasets (e.g., geophysical estimates of magma storage depth). One option is to use the spread of results from different H_2O-CO_2 solubility models as an indication of uncertainty (e.g., Wieser et al., 2025). However, as each model has different accuracy and precision for different melt compositions within their calibration range, the most appropriate model to use depends on the system of interest.

The most appropriate model to select can be evaluated by calculating accuracy (mean of the difference between calculated and known values) and precision (standard deviation of the difference between calculated and known values) of calculated P_{sat}^{v} and vapor composition using experiments that are close in composition to the system of interest (e.g., Wieser et al., 2025; Wieser, Kent, & Till, 2023). For instance, if one were interested in modelling a basaltic andesite with similar composition to Pavlof (Alaska, USA), you could calculate the accuracy and precision of P_{sat}^{v} using the experimental data of Mangan et al. (2021) (no measured vapor compositions are reported). This would require using the melt composition (including H_2O and CO_2), experimental conditions (*P* and *T*), and their uncertainties to calculate P_{sat}^{v} (and vapor composition) using different H_2O-CO_2 solubility models through a tool like VESIcal (or using the results from the calculations in this paper) and from this

calculating accuracy and precision. In this example, IaconoMarziano has -19% accuracy and 10% precision; ShishkinaIdealMixing 18% and 23%; and MagmaSat 2% and 16% for P_{sat}^{v}. This provides both an evidence-based choice and an assessment of uncertainty for the modelling results.

Conclusions

The accuracy and precision of five commonly-used H_2O-CO_2 solubility models (VolatileCalc-Basalt/Dixon, 1997/Newman & Lowenstern, 2002; MagamSat/Ghiorso & Gualda, 2015; Iacono-Marziano et al., 2012; Liu et al., 2005; Shishkina et al., 2014) were evaluated by calculating the vapor saturation pressure and composition using the Python packages VESIcal (Iacovino et al., 2021) and ThermoEngineLite (Wolf et al., 2026) on a literature dataset of 770 vapor-saturated silicate melt experiments with measured glass (and vapor) H_2O and CO_2 compositions. The calculated pressure of vapor saturation was compared to the experimental pressure, and the calculated vapor composition to reported vapor composition where available, for experimental data not used for calibration of each model. For the pressure of vapor saturation, models vary from being accurate across their stated calibration ranges (IaconoMarziano and MagmaSat) to quite inaccurate (Dixon, Shishkina, and Liu), and all are quite imprecise. Most models are accurate for the vapor composition (except ShishkinaIdealMixing) but all are relatively imprecise. The accuracy and precision can be better for different melt compositions within each models stated calibration range. For a system of interest, the most appropriate model can be chosen by evaluating the accuracy and precision for calculated vapor saturation pressure and composition when applied to experiments covering similar melt and *P-T* conditions, which is especially important when applying to natural data.

Acknowledgements

ECH was partially supported by the New Zealand Ministry of Business, Innovation and Employment (MBIE) through the Hazards and Risk Management (Strategic Science Investment Fund, contract C05X1702). Jon Blundy and Edward Stolper are thanked for their suggestions for experimental

studies that could be included in the compilation. Mark Ghiorso, Simon Matthews, and Sam Krasnof are thanked for their thoughts and advice on running MagmaSat using VESIcal.

Competing interests

The author declares no competing interests.

References

Aiuppa, A., Moretti, R., Federico, C., Giudice, G., Gurrieri, S., Liuzzo, M., Papale, P., Shinohara, H., & Valenza, M. (2007). Forecasting Etna eruptions by real-time observation of volcanic gas composition. *Geology*, *35*(12), 1115–1118. https://doi.org/10.1130/G24149A.1

Allison, C. M., Roggensack, K., & Clarke, A. B. (2019). H2O–CO2 solubility in alkali-rich mafic magmas: new experiments at mid-crustal pressures. *Contributions to Mineralogy and Petrology*, *174*(7), 58. https://doi.org/10.1007/s00410-019-1592-4

Alonso-Perez, R., Müntener, O., & Ulmer, P. (2008). Igneous garnet and amphibole fractionation in the roots of island arcs: experimental constraints on andesitic liquids. *Contributions to Mineralogy and Petrology 2008 157:4*, *157*(4), 541–558. https://doi.org/10.1007/S00410-008-0351-8

Anderson, A. T. J., Newman, S., Williams, S. N., Druitt, T. H., Skirius, C., & Stolper, E. M. (1989). H2O, CO2, Cl, and gas in Plinian and ash-flow Bishop rhyolite. *Geology*, *17*(3), 221–225. https://doi.org/10.1130/0091-7613(1989)017

Behrens, H., Misiti, V., Freda, C., Vetere, F., Botcharnikov, R. E., & Scarlato, P. (2009). Solubility of H2O and CO2 in ultrapotassic melts at 1200 and 1250 C and pressure from 50 to 500 MPa. *American Mineralogist*, *94*(1), 105–120. https://doi.org/10.2138/am.2009.2796

Behrens, H., Ohlhorst, S., Holtz, F., & Champenois, M. (2004). CO2 solubility in dacitic melts equilibrated with H2O-CO2 fluids: Implications for modeling the solubility of CO2 in silicic melts. *Geochimica et Cosmochimica Acta*, *68*(22), 4687–4703. https://doi.org/10.1016/J.GCA.2004.04.019

Behrens, H., Tamic, N., & Holtz, F. (2004). Determination of the molar absorption coefficient for the infrared absorption band of CO2 in rhyolitic glasses. *American Mineralogist*, *89*(2–3), 301–306. https://doi.org/10.2138/AM-2004-2-307

517 Blank, J. G., Stolper, E. M., & Carroll, M. R. (1993). Solubilities of carbon dioxide and water in rhyolitic
518 melt at 850°C and 750 bars. *Earth and Planetary Science Letters*, *119*(1–2), 27–36.
519 https://doi.org/10.1016/0012-821X(93)90004-S

520 Blatter, D. L., & Carmichael, I. S. E. (1998). Plagioclase-free andesites from Zitácuaro (Michoacán),
521 Mexico: Petrology and experimental constraints. *Contributions to Mineralogy and Petrology*,
522 *132*(2), 121–138. https://doi.org/10.1007/S004100050411/METRICS

523 Blatter, D. L., Sisson, T. W., & Hankins, W. Ben. (2013). Crystallization of oxidized, moderately hydrous
524 arc basalt at mid- to lower-crustal pressures: implications for andesite genesis. *Contributions to*
525 *Mineralogy and Petrology*, *166*(3), 861–886. https://doi.org/10.1007/s00410-013-0920-3

526 Blatter, D. L., Sisson, T. W., & Hankins, W. Ben. (2017). Voluminous arc dacites as amphibole reaction-
527 boundary liquids. *Contributions to Mineralogy and Petrology*, *172*(5), 27.
528 https://doi.org/10.1007/s00410-017-1340-6

529 Blatter, D. L., Sisson, T. W., & Hankins, W. Ben. (2023). Garnet stability in arc basalt, andesite, and
530 dacite—an experimental study. *Contributions to Mineralogy and Petrology 2023 178:6*, *178*(6),
531 33-. https://doi.org/10.1007/S00410-023-02008-W

532 Blundy, J. D., & Cashman, K. V. (2008). Petrologic reconstruction of magmatic system variables and
533 processes. *Reviews in Mineralogy and Geochemistry*, *69*(1), 179–239.
534 http://rimg.geoscienceworld.org/content/69/1/179

535 Botcharnikov, R. E., Behrens, H., & Holtz, F. (2006). Solubility and speciation of C–O–H fluids in
536 andesitic melt at T = 1100–1300 °C and P = 200 and 500 MPa. *Chemical Geology*, *229*(1–3),
537 125–143. https://doi.org/10.1016/J.CHEMGEO.2006.01.016

538 Botcharnikov, R. E., Freise, M., Holtz, F., & Behrens, H. (2005). Solubility of COH mixtures in natural
539 melts: new experimental data and application range of recent models. *Annals of Geophysics*,
540 *48*(4–5), 633–646.

541 Botcharnikov, R. E., Holtz, F., & Behrens, H. (2007). The effect of CO2 on the solubility of H2O-Cl fluids
542 in andesitic melt. *European Journal of Mineralogy*, *19*(5), 671–680.
543 https://doi.org/10.1127/0935-1221/2007/0019-1752

544 Burgisser, A., Alletti, M., & Scaillet, B. (2015). Simulating the behavior of volatiles belonging to the C–
545 O–H–S system in silicate melts under magmatic conditions with the software D-Compress.
546 *Computers & Geosciences*, *79*, 1–14. https://doi.org/10.1016/J.CAGEO.2015.03.002

547 Ding, S., Plank, T., Wallace, P. J., & Rasmussen, D. J. (2023). Sulfur_X: A Model of Sulfur Degassing
548 During Magma Ascent. *Geochemistry, Geophysics, Geosystems*, *24*(4), e2022GC010552.
549 https://doi.org/10.1029/2022GC010552

550 Dixon, J. E. (1997). Degassing of alkalic basalts. *American Mineralogist*, *82*(3–4), 368–378.
551 https://doi.org/10.2138/AM-1997-3-415

552 Dixon, J. E., & Stolper, E. M. (1995). An experimental study water and carbon dioxide solubilities in
553 mid-ocean ridge basaltic liquids. Part II: Application to degassing. *Journal of Petrology*, *36*(6),
554 1633–1646.

555 Dixon, J. E., Stolper, E. M., & Holloway, J. R. (1995). An experimental study of water and carbon
556 dioxide solubilities in mid-ocean ridge basaltic liquids. Part I: Calibration and solubility models.
557 *Journal of Petrology*, *36*(6), 1607–1631.
558 https://doi.org/10.1093/oxfordjournals.petrology.a037267

559 Duan, X. (2014). A general model for predicting the solubility behavior of H2O–CO2 fluids in silicate
560 melts over a wide range of pressure, temperature and compositions. *Geochimica et*
561 *Cosmochimica Acta*, *125*, 582–609. https://doi.org/10.1016/J.GCA.2013.10.018

562 Edmonds, M., Bouvier, A.-S., Hughes, E., Iacovino, K., & Shahar, A. (n.d.). Part 1: Tectonics and
563 Plumbing Systems - Magmatic volatiles and their role in magma ascent and degassing. In C.
564 Bonadonna, Lc. A. Caricchi, P. Cole, J. Lindsay, J. Lowenstern, R. Robertson, & M. L. Villegas
565 (Eds.), *Encylopedia of Volcanoes* (third, 2.2). Elsevier.

566 Fanara, S., Botcharnikov, R. E., Palladino, D. M., Adams, F., Buddensieck, J., Mulch, A., & Behrens, H.
567 (2015). Volatiles in magmas related to the Campanian Ignimbrite eruption: Experiments vs.
568 natural findings. *American Mineralogist*, *100*(10), 2284–2297. https://doi.org/10.2138/AM-
569 2015-5033

570 Feig, S. T., Koepke, J., & Snow, J. E. (2006). Effect of water on tholeiitic basalt phase equilibria: an
571 experimental study under oxidizing conditions. *Contributions to Mineralogy and Petrology*,
572 *152*(5), 611–638. https://doi.org/10.1007/s00410-006-0123-2

573 Fogel, R. A., & Rutherford, M. J. (1990). The solubility of carbon dioxide in rhyolitic melts; a
574 quantitative FTIR study. *American Mineralogist*, *75*(11–12), 1311–1326.

575 Ghiorso, M. S., & Gualda, G. A. R. (2015). An H2O–CO2 mixed fluid saturation model compatible with
576 rhyolite-MELTS. *Contributions to Mineralogy and Petrology*, *169*(6), 53.
577 https://doi.org/10.1007/s00410-015-1141-8

578 Giordano, D., Russell, J. K., & Dingwell, D. B. (2008). Viscosity of magmatic liquids: A model. *Earth and*
579 *Planetary Science Letters*, *271*(1), 123–134.
580 http://www.sciencedirect.com/science/article/pii/S0012821X08002240

581 Hartley, M. E., Maclennan, J., Edmonds, M., & Thordarson, T. (2014). Reconstructing the deep CO2
582 degassing behaviour of large basaltic fissure eruptions. *Earth and Planetary Science Letters*, *393*,
583 120–131. https://doi.org/10.1016/j.epsl.2014.02.031

584 Hughes, E. C., Buse, B., Kearns, S. L., Blundy, J. D., Kilgour, G., Mader, H. M., Brooker, R. A., Blazer, B.,
585 Botcharnikov, R. E., Di Genova, D., Almeev, R. R., & Riker, J. M. (2018). High spatial resolution
586 analysis of the Iron oxidation state in silicate glasses using the electron probe. *American*
587 *Mineralogist*, *103*, 1473–1486.

588 Hughes, E. C., Law, S., Kilgour, G., Blundy, J. D., & Mader, H. M. (2023). Storage, evolution, and mixing
589 in basaltic eruptions from around the Okataina Volcanic Centre, Taupō Volcanic Zone, Aotearoa
590 New Zealand. *Journal of Volcanology and Geothermal Research*, *434*, 107715.
591 https://doi.org/10.1016/J.JVOLGEORES.2022.107715

592 Hughes, E. C., Liggins, P., Saper, L., & Stolper, E. M. (2024). The effects of oxygen fugacity and sulfur
593 on the pressure of vapor-saturation of magma. *American Mineralogist*, *109*, 422–438.

594 Hughes, E. C., Liggins, P., Wieser, P., & Stolper, E. M. (2025). VolFe: an open-source Python package
595 for calculating melt-vapour equilibria including silicate melt, carbon, hydrogen, sulfur, and noble
596 gases. *Volcanica*, *8*(2), 457–-481. https://doi.org/10.30909/vol/imvc1781

597 Iacono Marziano, G., Gaillard, F., & Pichavant, M. (2007). Limestone assimilation by basaltic magmas:
598 an experimental re-assessment and application to Italian volcanoes. *Contributions to*
599 *Mineralogy and Petrology 2007 155:6*, *155*(6), 719–738. https://doi.org/10.1007/S00410-007-
600 0267-8

601 Iacono-Marziano, G., Morizet, Y., Le Trong, E., & Gaillard, F. (2012). New experimental data and semi-
602 empirical parameterization of H2O–CO2 solubility in mafic melts. *Geochimica et Cosmochimica*
603 *Acta*, *97*, 1–23. https://doi.org/10.1016/J.GCA.2012.08.035

604 Iacovino, K., Matthews, S., Wieser, P. E., Moore, G. M., & Bégué, F. (2021). VESIcal Part I: An open-
605 source thermodynamic model engine for mixed volatile (O-) solubility in silicate melts. *Earth*
606 *and Space Science*, e2020EA001584. https://doi.org/10.1029/2020EA001584

607 Iacovino, K., Moore, G., Roggensack, K., Oppenheimer, C., & Kyle, P. (2013). H2O–CO2 solubility in
608 mafic alkaline magma: applications to volatile sources and degassing behavior at Erebus

609 volcano, Antarctica. *Contributions to Mineralogy and Petrology 2013 166:3*, *166*(3), 845–860.
610 https://doi.org/10.1007/S00410-013-0877-2

611 Jakobsson, S. (1997). Solubility of water and carbon dioxide in an icelandite at 1400 °C and 10
612 kilobars. *Contributions to Mineralogy and Petrology 1997 127:1*, *127*(1), 129–135.
613 https://doi.org/10.1007/S004100050270

614 Jendrzejewski, N., Trull, T. W., Pineau, F., & Javoy, M. (1997). Carbon solubility in Mid-Ocean Ridge
615 basaltic melt at low pressures (250–1950 bar). *Chemical Geology*, *138*(1–2), 81–92.
616 https://doi.org/10.1016/S0009-2541(96)00176-3

617 Jiménez-Mejías, M., Andújar, J., Scaillet, B., & Casillas, R. (2022). Experimental determination of H2O
618 and CO2 solubilities of mafic alkaline magmas from Canary Islands. *Comptes Rendus.*
619 *Géoscience*, *353*(S2), 289–314. https://doi.org/10.5802/crgeos.84

620 Kern, C., Aiuppa, A., & de Moor, J. M. (2022). A golden era for volcanic gas geochemistry? *Bulletin of*
621 *Volcanology 2022 84:5*, *84*(5), 1–11. https://doi.org/10.1007/S00445-022-01556-6

622 Kilgour, G., Blundy, J., Cashman, K., & Mader, H. M. (2013). Small volume andesite magmas and melt-
623 mush interactions at Ruapehu, New Zealand: Evidence from melt inclusions. *Contributions to*
624 *Mineralogy and Petrology*, *166*(2), 371–392. https://doi.org/10.1007/S00410-013-0880-
625 7/FIGURES/11

626 King, P. L., & Holloway, J. R. (2002). CO2 solubility and speciation in intermediate (andesitic) melts:
627 the role of H2O and composition. *Geochimica et Cosmochimica Acta*, *66*(9), 1627–1640.
628 https://doi.org/10.1016/S0016-7037(01)00872-9

629 Krawczynski, M. J., Grove, T. L., & Behrens, H. (2012). Amphibole stability in primitive arc magmas:
630 effects of temperature, H2O content, and oxygen fugacity. *Contributions to Mineralogy and*
631 *Petrology 2012 164:2*, *164*(2), 317–339. https://doi.org/10.1007/S00410-012-0740-X

632 La Spina, G., Arzilli, F., Burton, M. R., Polacci, M., & Clarke, A. B. (2022). Role of volatiles in highly
633 explosive basaltic eruptions. *Communications Earth & Environment 2022 3:1*, *3*(1), 156-.
634 https://doi.org/10.1038/s43247-022-00479-6

635 Lesne, P., Kohn, S. C., Blundy, J. D., Witham, F., Botcharnikov, R. E., & Behrens, H. (2011).
636 Experimental Simulation of Closed-System Degassing in the System Basalt-H2O-CO2-S-Cl.
637 *Journal of Petrology*, *52*(9), 1737–1762. https://doi.org/10.1093/petrology/egr027

638 Lesne, P., Scaillet, B., Pichavant, M., & Brey, G. P. (2011). The carbon dioxide solubility in alkali basalts:
639 an experimental study. *Contributions to Mineralogy and Petrology*, *162*(1), 153–168.
640 https://doi.org/10.1007/s00410-010-0585-0

641 Lesne, P., Scaillet, B., Pichavant, M., Iacono-Marziano, G., & Beny, J. M. (2011). The H2O solubility of
642 alkali basaltic melts: An experimental study. *Contributions to Mineralogy and Petrology*, *162*(1),
643 133–151. https://doi.org/10.1007/S00410-010-0588-X/FIGURES/12

644 Liggins, P., Shorttle, O., & Rimmer, P. B. (2020). Can volcanism build hydrogen-rich early
645 atmospheres? *Earth and Planetary Science Letters*, *550*, 116546.
646 https://doi.org/10.1016/J.EPSL.2020.116546

647 Liu, Y., Zhang, Y., & Behrens, H. (2005). Solubility of H2O in rhyolitic melts at low pressures and a new
648 empirical model for mixed H2O–CO2 solubility in rhyolitic melts. *Journal of Volcanology and*
649 *Geothermal Research*, *143*(1–3), 219–235. https://doi.org/10.1016/J.JVOLGEORES.2004.09.019

650 Mangan, M. T., & Sisson, T. (2000). Delayed, disequilibrium degassing in rhyolite magma:
651 decompression experiments and implications for explosive volcanism. *Earth and Planetary*
652 *Science Letters*, *183*(3–4), 441–455. https://doi.org/10.1016/S0012-821X(00)00299-5

653 Mangan, M. T., Sisson, T. W., Hankins, W. Ben, Shimizu, N., & Vennemann, T. (2021). Constraints on
654 deep, CO2-rich degassing at arc volcanoes from solubility experiments on hydrous basaltic
655 andesite of Pavlof Volcano, Alaska Peninsula, at 300 to 1200 MPa. *American Mineralogist*,
656 *106*(5), 762–773. https://doi.org/10.2138/am-2021-7531

657 Marxer, F., Ulmer, P., & Müntener, O. (2021). Polybaric fractional crystallisation of arc magmas: an
658 experimental study simulating trans-crustal magmatic systems. *Contributions to Mineralogy and*
659 *Petrology 2021 177:1*, *177*(1), 3-. https://doi.org/10.1007/S00410-021-01856-8

660 Mastin, L. G. (2002). Insights into volcanic conduit flow from an open-source numerical model.
661 *Geochemistry, Geophysics, Geosystems*, *3*(7), 1–18. https://doi.org/10.1029/2001GC000192

662 Melekhova, E., Blundy, J., Martin, R., Arculus, R., & Pichavant, M. (2017). Petrological and
663 experimental evidence for differentiation of water-rich magmas beneath St. Kitts, Lesser
664 Antilles. *Contributions to Mineralogy and Petrology*, *172*(11–12), 98.
665 https://doi.org/10.1007/s00410-017-1416-3

666 Moore, L. R., Gazel, E., Tuohy, R., Lloyd, A. S., Esposito, R., Steele-MacInnis, M., Hauri, E. H., Wallace,
667 P. J., Plank, T., & Bodnar, R. J. (2015). Bubbles matter: An assessment of the contribution of

668 vapor bubbles to melt inclusion volatile budgets. *American Mineralogist*, *100*(4), 806–823.
669 https://doi.org/10.2138/am-2015-5036

670 Moretti, R., Papale, P., & Ottonello, G. (2003). A model for the saturation of C-O-H-S fluids in silicate
671 melts. *Geological Society, London, Special Publications*, *213*(1), 81–101.
672 https://doi.org/10.1144/GSL.SP.2003.213.01.06

673 Nandedkar, R. H., Ulmer, P., & Müntener, O. (2014). Fractional crystallization of primitive, hydrous arc
674 magmas: An experimental study at 0.7 GPa. *Contributions to Mineralogy and Petrology*, *167*(6),
675 1–27. https://doi.org/10.1007/s00410-014-1015-5

676 Newman, S., & Lowenstern, J. B. (2002). VolatileCalc: a silicate melt–H2O–CO2 solution model
677 written in Visual Basic for excel. *Computers & Geosciences*, *28*(5), 597–604.
678 https://doi.org/10.1016/S0098-3004(01)00081-4

679 Papale, P., Moretti, R., & Barbato, D. (2006). The compositional dependence of the saturation surface
680 of H2O+CO2 fluids in silicate melts. *Chemical Geology*, *229*(1), 78–95.
681 https://doi.org/10.1016/j.chemgeo.2006.01.013

682 Papale, P., Moretti, R., & Paonita, A. (2022). Thermodynamics of Multi-component Gas–Melt
683 Equilibrium in Magmas: Theory, Models, and Applications. *Reviews in Mineralogy and*
684 *Geochemistry*, *87*(1), 431–556. https://doi.org/10.2138/RMG.2022.87.10

685 Pawley, A. R., Holloway, J. R., & McMillan, P. F. (1992). The effect of oxygen fugacity on the solubility
686 of carbon-oxygen fluids in basaltic melt. *Earth and Planetary Science Letters*, *110*(1–4), 213–
687 225. https://doi.org/10.1016/0012-821X(92)90049-2

688 Rasmussen, D. J., Plank, T. A., Wallace, P. J., Newcombe, M. E., & Lowenstern, J. B. (2020). Vapor-
689 bubble growth in olivine-hosted melt inclusions. *American Mineralogist*, *105*(12), 1898–1919.
690 https://doi.org/10.2138/am-2020-7377

691 Riker, J. M., Blundy, J. D., Rust, A. C., Botcharnikov, R. E., & Humphreys, M. C. S. (2015). Experimental
692 phase equilibria of a Mount St. Helens rhyodacite: A framework for interpreting crystallization
693 paths in degassing silicic magmas. *Contributions to Mineralogy and Petrology*, *170*(6).
694 https://doi.org/doi:10.1007/s00410-015-1160-5

695 Rose-Koga, E. F., Bouvier, A. S., Gaetani, G. A., Wallace, P. J., Allison, C. M., Andrys, J. A., Angeles de la
696 Torre, C. A., Barth, A., Bodnar, R. J., Bracco Gartner, A. J. J., Butters, D., Castillejo, A., Chilson-
697 Parks, B., Choudhary, B. R., Cluzel, N., Cole, M., Cottrell, E., Daly, A., Danyushevsky, L. V., … Zhou,
698 T. (2021). Silicate melt inclusions in the new millennium: A review of recommended practices

for preparation, analysis, and data presentation. *Chemical Geology*, *570*, 120145. https://doi.org/10.1016/j.chemgeo.2021.120145

Schanofski, M., Fanara, S., & Schmidt, B. C. (2019). CO2–H2O solubility in K-rich phonolitic and leucititic melts. *Contributions to Mineralogy and Petrology*, *174*(6), 52. https://doi.org/10.1007/s00410-019-1581-7

Shea, J., Hughes, E., Balzer, R., Bindeman, I., Blundy, J., Brooker, R., Botcharnikov, R., Cartigny, P., Gaetani, G., Kilgour, G., Maclennan, J., Monteleone, B., Neave, D. A., & Shorttle, O. (2025). Improved Precision and Reference Materials for Stable Carbon Isotope Measurement in Basaltic Glasses using Secondary Ion Mass Spectrometry. *Geostandards and Geoanalytical Research*, *49*(3), 607–627. https://doi.org/10.1111/GGR.12609;WGROUP:STRING:PUBLICATION

Shishkina, T. A., Botcharnikov, R. E., Holtz, F., Almeev, R. R., Jazwa, A. M., & Jakubiak, A. A. (2014). Compositional and pressure effects on the solubility of H2O and CO2 in mafic melts. *Chemical Geology*, *388*, 112–129. https://doi.org/10.1016/J.CHEMGEO.2014.09.001

Shishkina, T. A., Botcharnikov, R. E., Holtz, F., Almeev, R. R., & Portnyagin, M. V. (2010). Solubility of H2O- and CO2-bearing fluids in tholeiitic basalts at pressures up to 500 MPa. *Chemical Geology*, *277*(1–2), 115–125. https://doi.org/10.1016/J.CHEMGEO.2010.07.014

Stanley, B. D., Hirschmann, M. M., & Withers, A. C. (2011). CO2 solubility in Martian basalts and Martian atmospheric evolution. *Geochimica et Cosmochimica Acta*, *75*(20), 5987–6003. https://doi.org/10.1016/J.GCA.2011.07.027

Stanley, B. D., Schaub, D. R., & Hirschmann, M. M. (2012). CO2 solubility in primitive martian basalts similar to Yamato 980459, the effect of composition on CO2 solubility of basalts, and the evolution of the martian atmosphere. *American Mineralogist*, *97*(11–12), 1841–1848. https://doi.org/10.2138/AM.2012.4141

Stolper, E. M., & Holloway, J. R. (1988). Experimental determination of the solubility of carbon dioxide in molten basalt at low pressure. *Earth and Planetary Science Letters*, *87*(397–408).

Sun, C., & Lee, C.-T. A. (2022). Redox evolution of crystallizing magmas with C-H-O-S volatiles and its implications for atmospheric oxygenation. *Geochimica et Cosmochimica Acta*, *338*, 302–321.

Tamic, N., Behrens, H., & Holtz, F. (2001). The solubility of H2O and CO2 in rhyolitic melts in equilibrium with a mixed CO2–H2O fluid phase. *Chemical Geology*, *174*(1–3), 333–347. https://doi.org/10.1016/S0009-2541(00)00324-7

van Gerve, T. D., Namur, O., & Borst, A. (2025). Constraining the Impact of Post-Entrapment Crystallization Correction Algorithms on Melt Inclusion Compositions and Petrological Interpretations With MagmaPEC. *Geochemistry, Geophysics, Geosystems*, *26*(10), e2025GC012420. https://doi.org/10.1029/2025GC012420;REQUESTEDJOURNAL:JOURNAL:15252027;WEBSITE:WEBSITE:AGUPUBS;ISSUE:ISSUE:DOI

Vetere, F., Botcharnikov, R. E., Holtz, F., Behrens, H., & De Rosa, R. (2011). Solubility of H2O and CO2 in shoshonitic melts at 1250°C and pressures from 50 to 400MPa: Implications for Campi Flegrei magmatic systems. *Journal of Volcanology and Geothermal Research*, *202*(3–4), 251–261. https://doi.org/10.1016/j.jvolgeores.2011.03.002

Vetere, F., Holtz, F., Behrens, H., Botcharnikov, R. E., & Fanara, S. (2014). The effect of alkalis and polymerization on the solubility of H2O and CO2 in alkali-rich silicate melts. *Contributions to Mineralogy and Petrology*, *167*(5), 1014. https://doi.org/10.1007/s00410-014-1014-6

Wallace, P. J., Kamenetsky, V. S., & Cervantes, P. (2015). Melt inclusion CO2 contents, pressures of olivine crystallization, and the problem of shrinkage bubbles. *American Mineralogist*, *100*(4), 787–794. https://doi.org/10.2138/am-2015-5029

Wallace, P. J., Plank, T., Edmonds, M., & Hauri, E. H. (2015). Volatiles in Magmas. *The Encyclopedia of Volcanoes*, 163–183. https://doi.org/10.1016/B978-0-12-385938-9.00007-9

Wieser, P. E., Gleeson, M. L. M., Matthews, S., DeVitre, C., & Gazel, E. (2025). Determining the pressure-temperature-composition (P-T-X) conditions of magma storage. *Treatise on Geochemistry, Third Edition, 8 Volume Set*, *2*, 83–151. https://doi.org/10.1016/B978-0-323-99762-1.00024-3

Wieser, P. E., Iacovino, K., Matthews, S., Moore, G., & Allison, C. M. (2022). VESIcal: 2. A Critical Approach to Volatile Solubility Modeling Using an Open-Source Python3 Engine. *Earth and Space Science*, *9*(2), e2021EA001932. https://doi.org/10.1029/2021EA001932

Wieser, P. E., Kent, A. J. R., & Till, C. B. (2023). Barometers Behaving Badly II: a Critical Evaluation of Cpx-Only and Cpx-Liq Thermobarometry in Variably-Hydrous Arc Magmas. *Journal of Petrology*, *64*(8). https://doi.org/10.1093/PETROLOGY/EGAD050

Wieser, P. E., Kent, A. J. R., Till, C. B., & Abers, G. A. (2023). Geophysical and Geochemical Constraints on Magma Storage Depths Along the Cascade Arc: Knowns and Unknowns. *Geochemistry,*

759 *Geophysics, Geosystems*, *24*(11), e2023GC011025.
760 https://doi.org/10.1029/2023GC011025;PAGE:STRING:ARTICLE/CHAPTER

761 Wolf, A. S., Matthews, S. W., Birner, S., & Ghiorso, M. S. (2026). *ThermoEngineLite* (2.0.0.dev7).
762 Zenodo. https://doi.org/10.5281/zenodo.19715236

763 Yoshimura, S. (2023). Carbon dioxide and water in the crust. Part 2: Solubility in silicate melts. *Journal*
764 *of Mineralogical and Petrological Sciences*, *118*(1), 221224b.
765 https://doi.org/10.2465/JMPS.221224B

766